Electronic Supplementary Material (ESI) for Journal of Materials Chemistry C.
This journal is © The Royal Society of Chemistry 2016

Supporting Information

Novel pyrene containing monomeric and dimeric supramolecular AIEE active nano-probes utilized in selective "off-on" trivalent metal and highly acidic pH sensing with live cell applications

Muthaiah Shellaiah,[a] Turibius Simon,[b] Venkatesan Srinivasadesikan,[c] Chein-Min Lin,[d] Kien Wen Sun,[a,d*] Fu-Hsiang Ko,[b] Ming-Chang Lin[c] and Hong-Cheu Lin[b]

*[a]Department of Applied Chemistry, National Chiao Tung University, Hsinchu 300, Taiwan.

[b]Department of Materials Science and Engineering, National Chiao Tung University, Hsinchu 300, Taiwan.

[c]Center for Interdisciplinary Molecular Science, Department of Applied Chemistry, National Chiao Tung University, Hsinchu 300, Taiwan.

[d]Department of Electronics Engineering, National Chiao Tung University, Hsinchu 300, Taiwan.

E-mail: kwsun@mail.nctu.edu.tw

Table of contents:

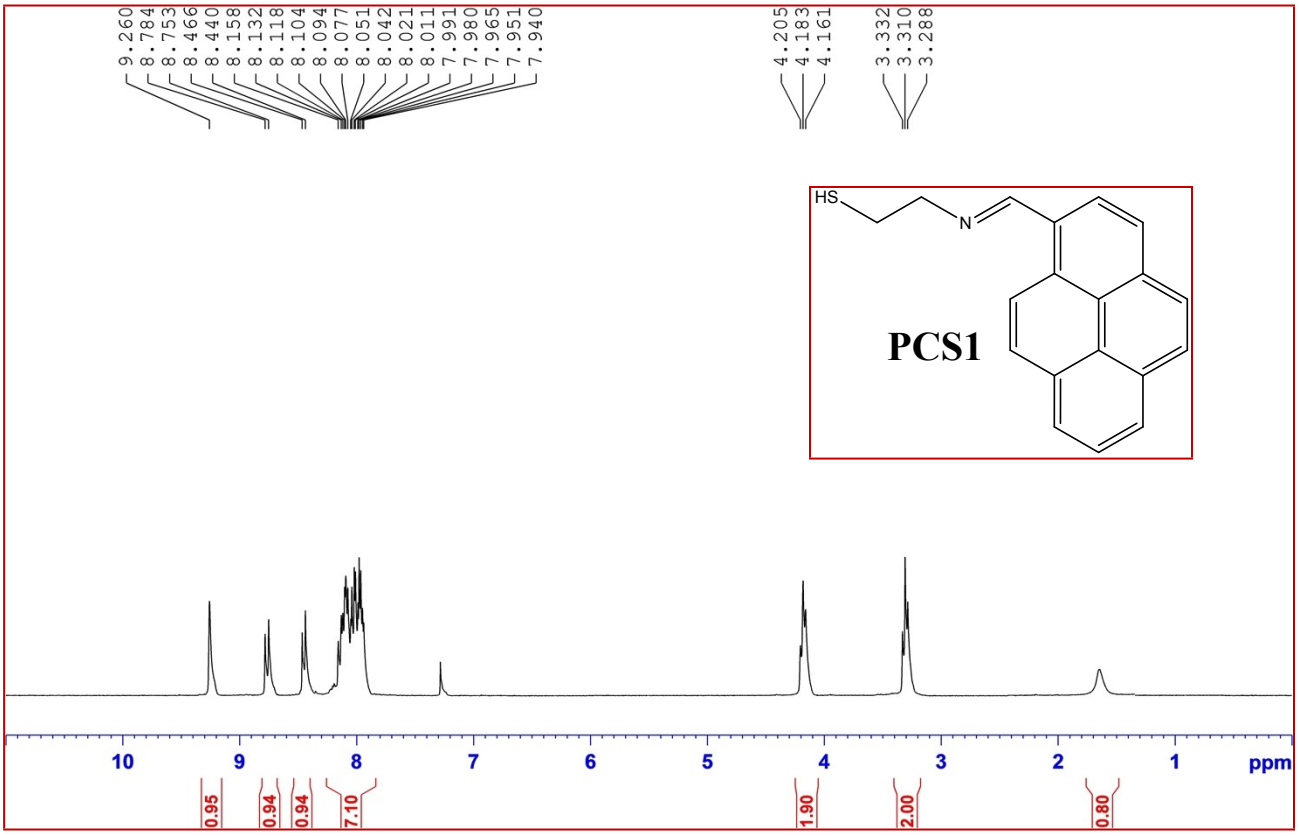

Fig. S1 ^{1}H NMR spectrum of **PCS1** in $CDCl_3$.

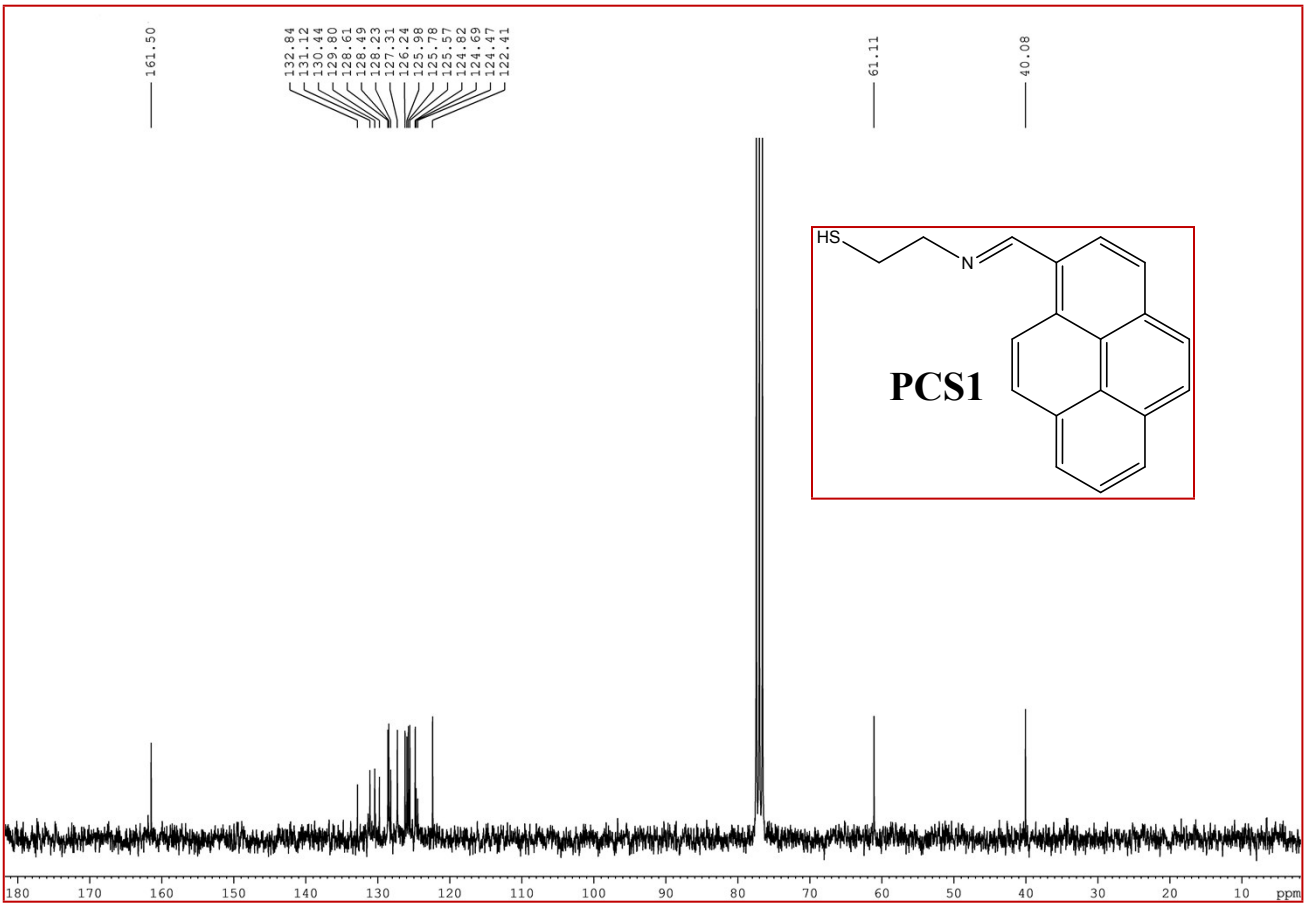

Fig. S2 ^{13}C NMR spectrum of **PCS1** in $CDCl_3$.

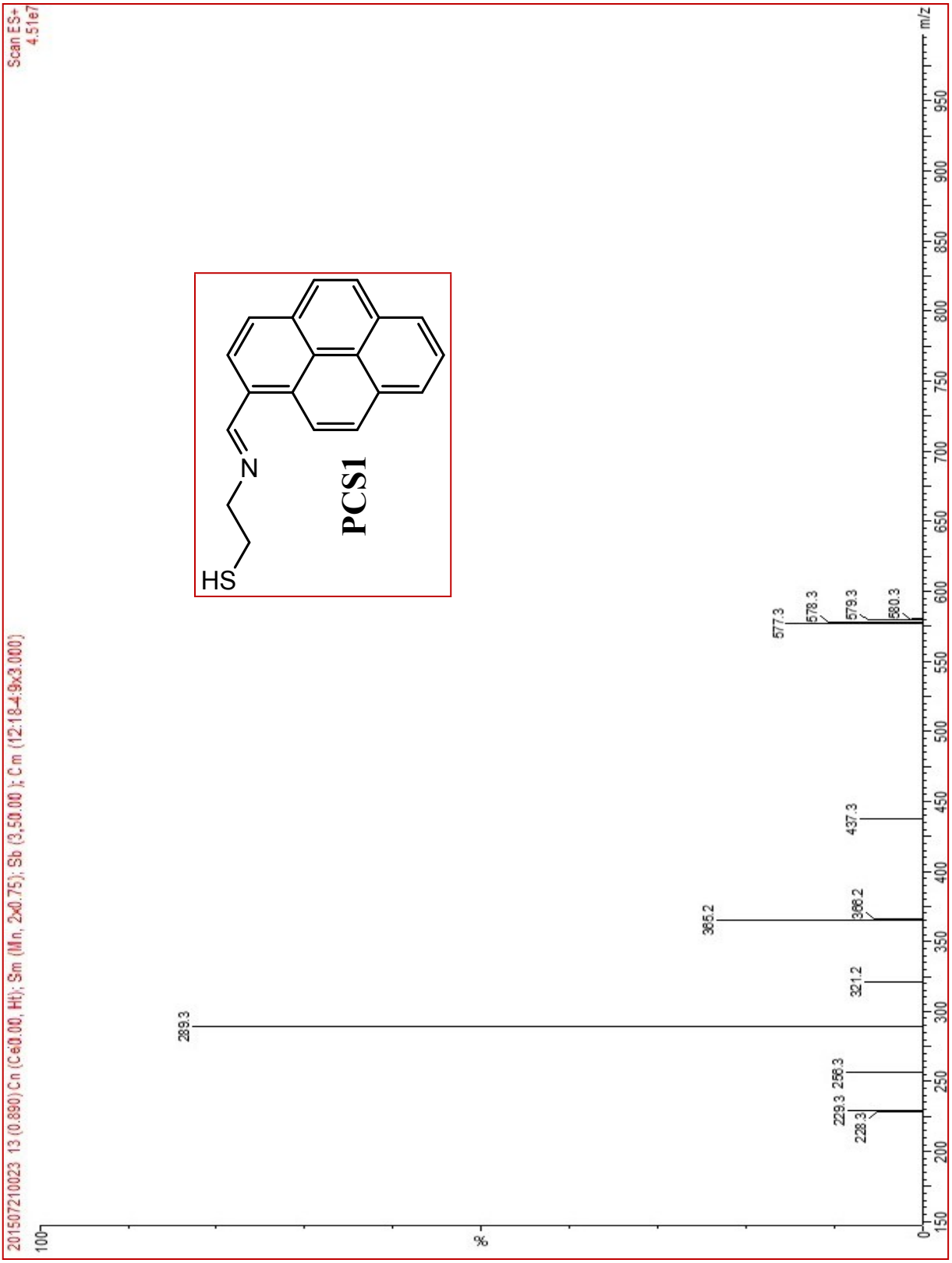

Fig. S3 ESI (+Ve) Mass spectrum of **PCS1**.

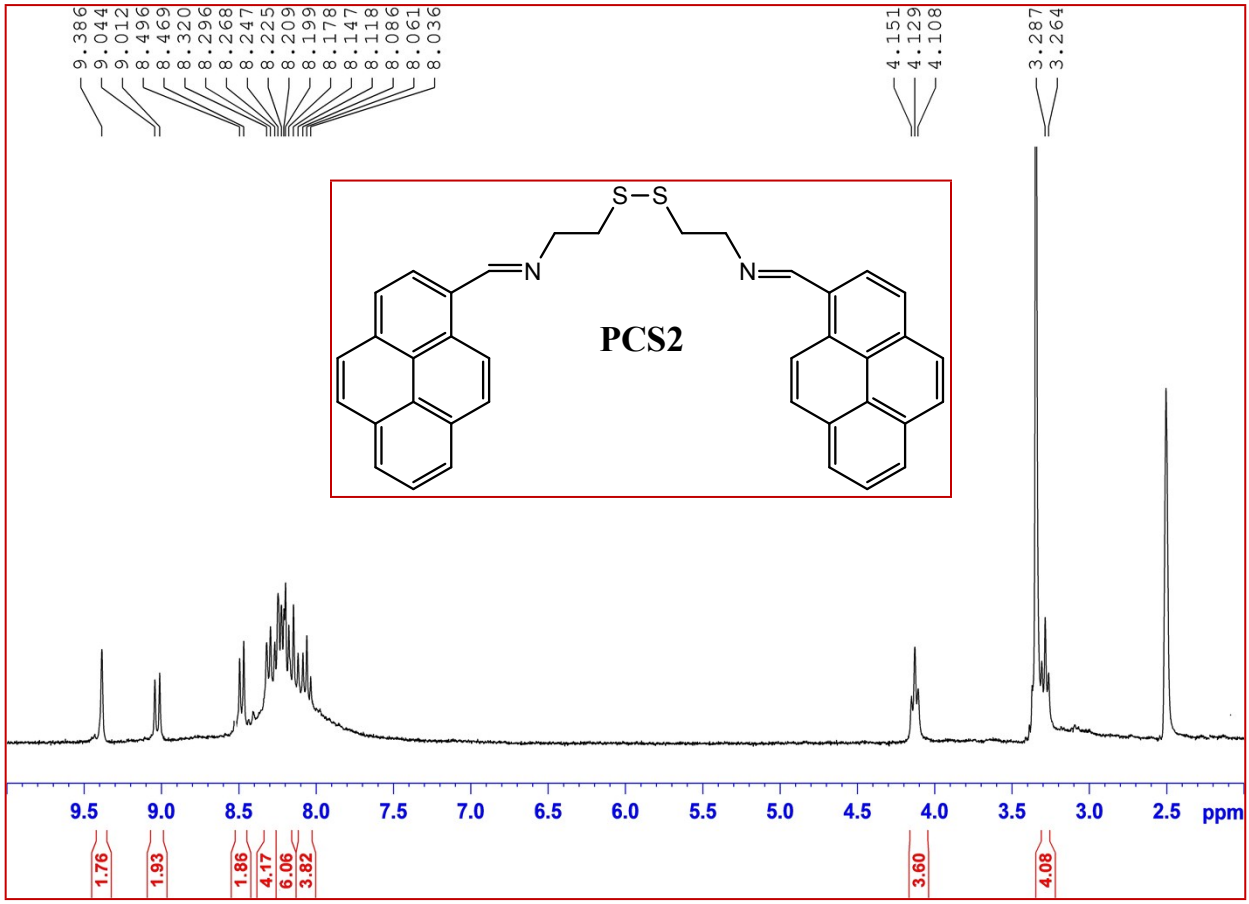

Fig. S4 ^{1}H NMR spectrum of **PCS2** in d_6-DMSO.

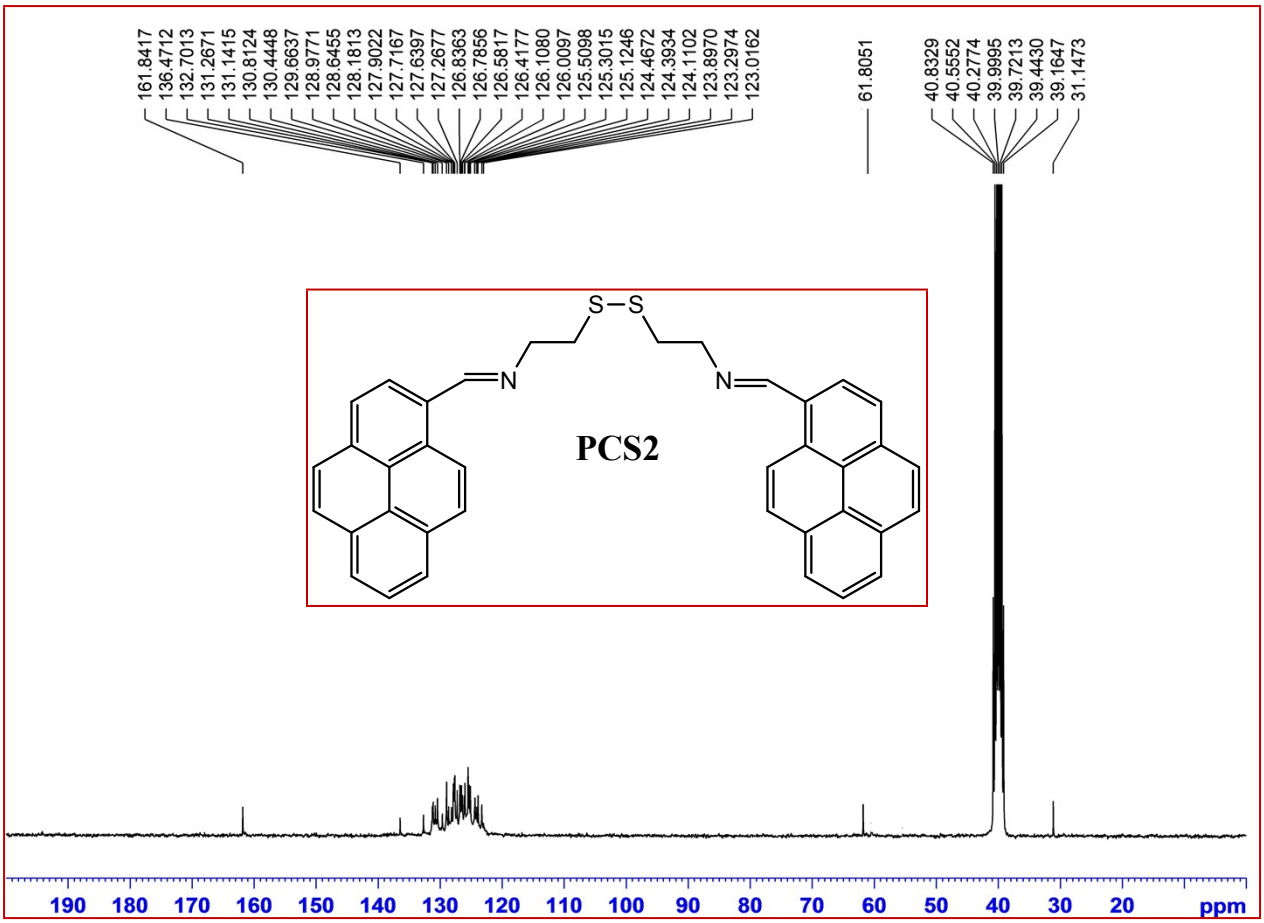

Fig. S5 ^{13}C NMR spectrum of **PCS2** in d_6-DMSO.

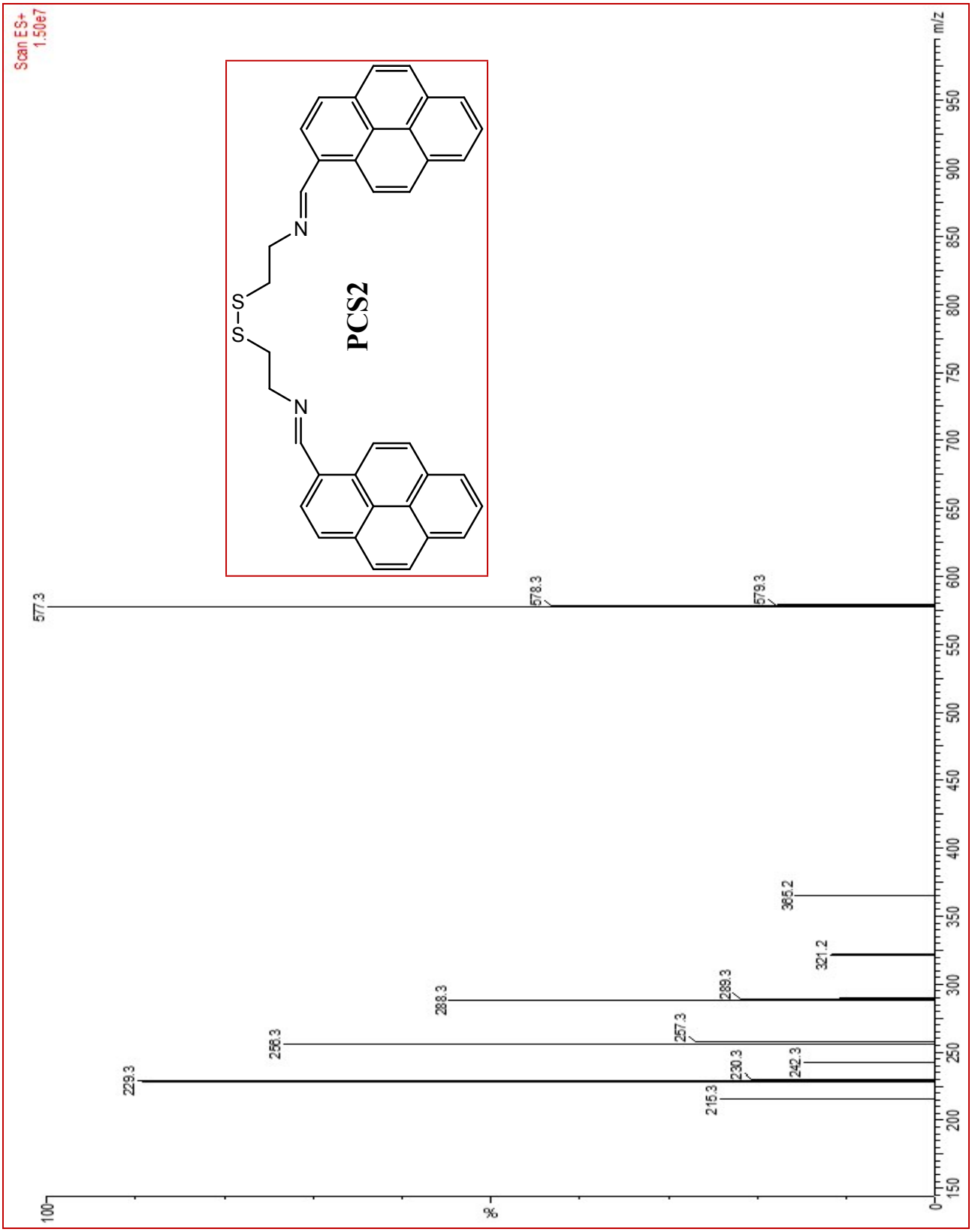

Fig. S6 ESI (+Ve) Mass spectrum of **PCS2**.

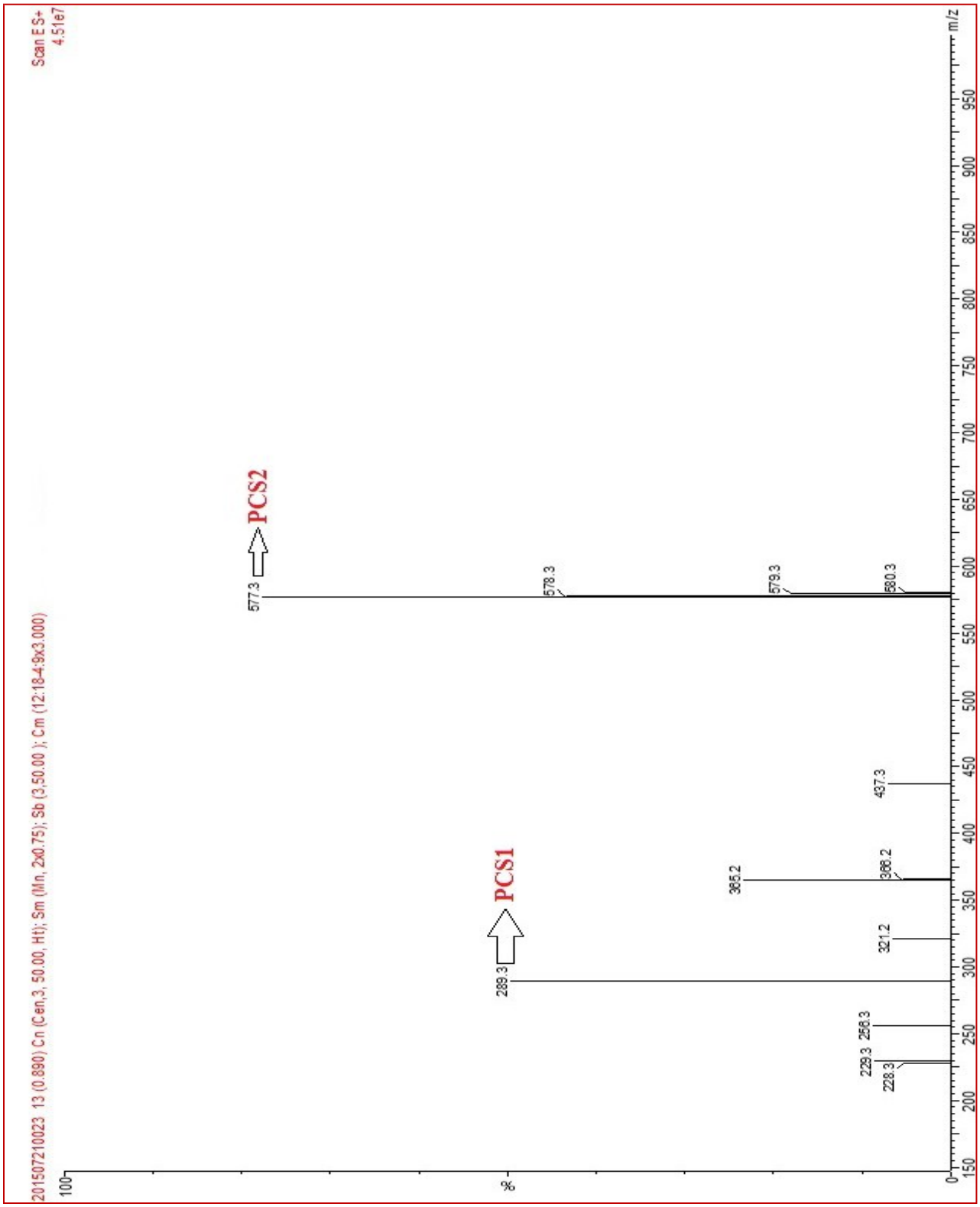

Fig. S7 ESI (+Ve) Mass spectrum of **PCS1** in 1M NaOH solution.

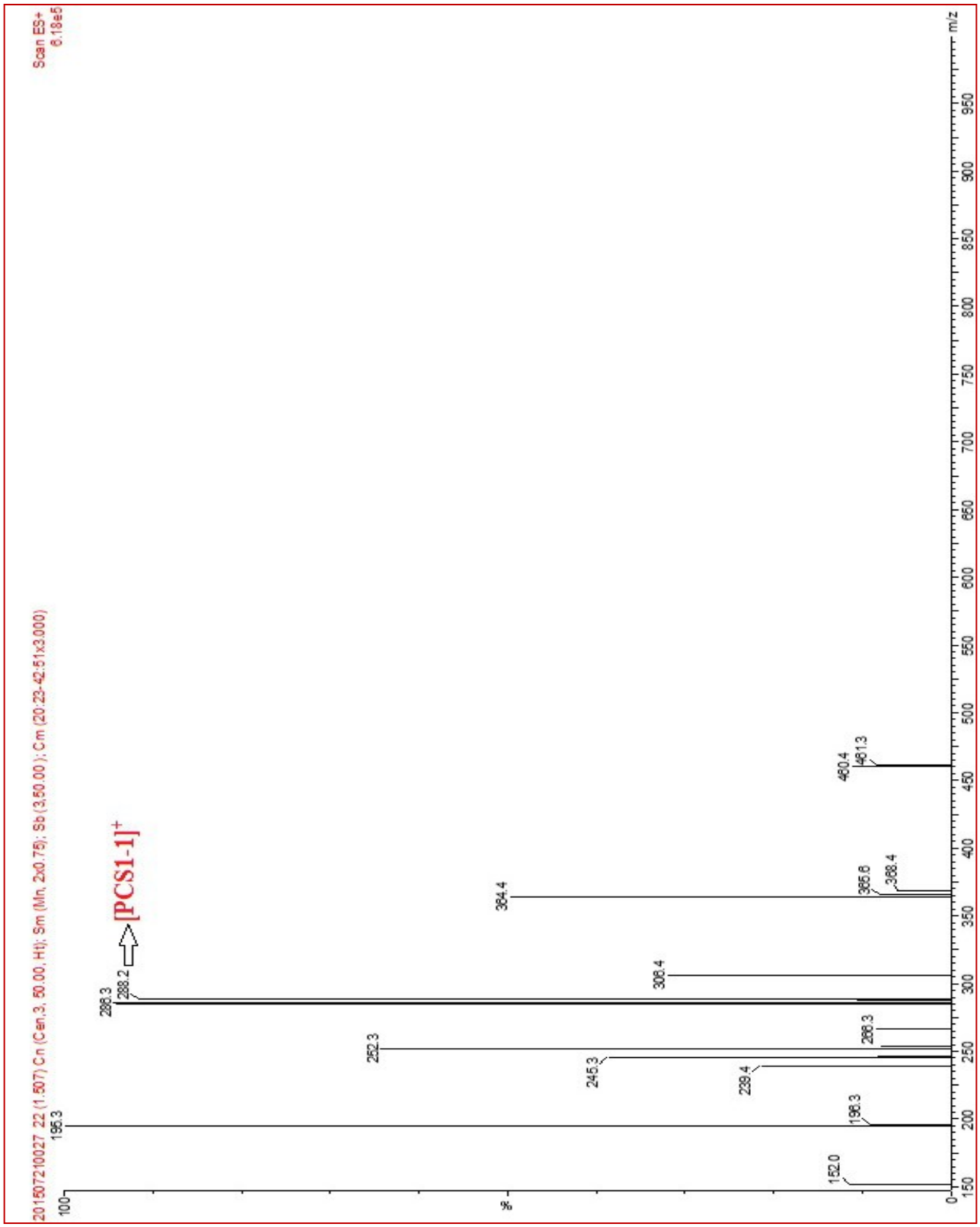

Fig. S8 ESI (+Ve) Mass spectrum of **PCS2** + HCl (100 µl; 1M) complex.

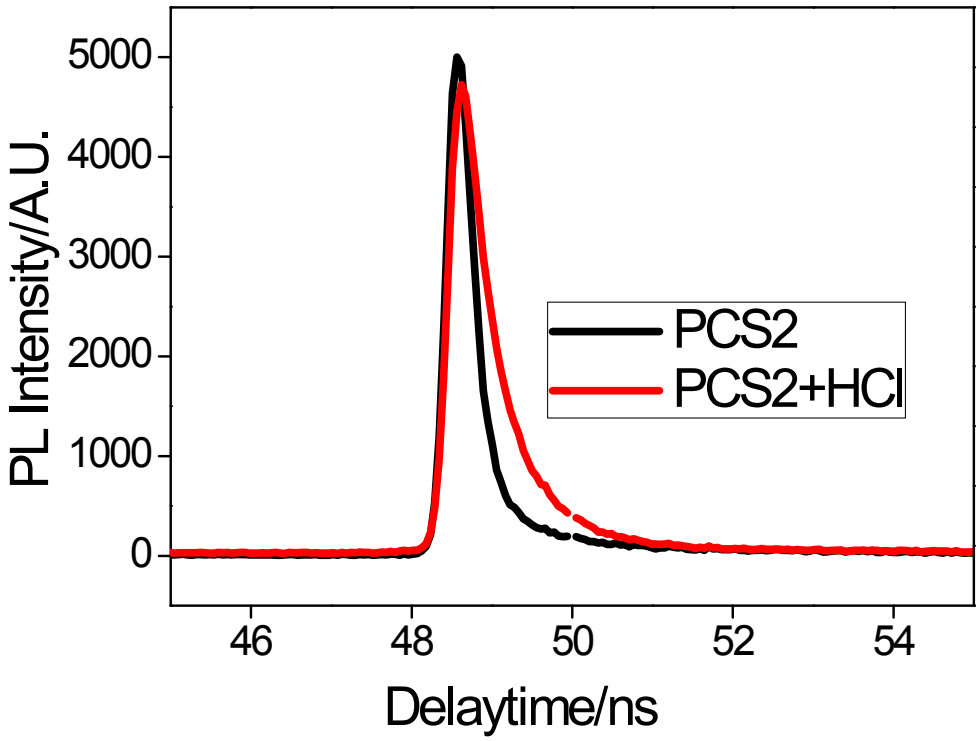

Fig. S9 TRPL spectra of **PCS2** and **PCS2** + HCl (20 μl; 1M) in DMSO solution.

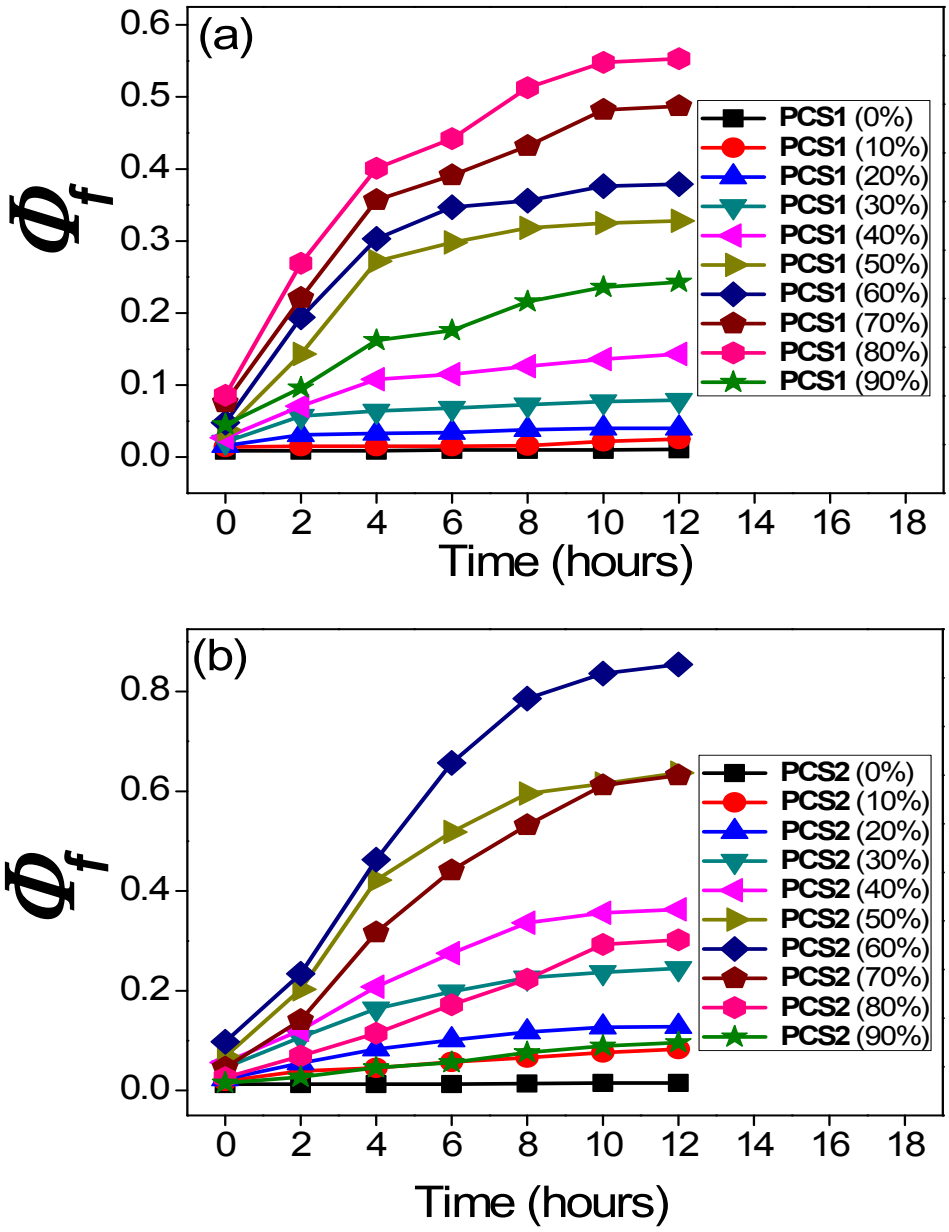

Fig. S10 Quantum yield (Φ_f) changes of (a) **PCS1** and (b) **PCS2**, upon increasing the concentration of water fraction (0-90%) as a function of time (0-12 hours).

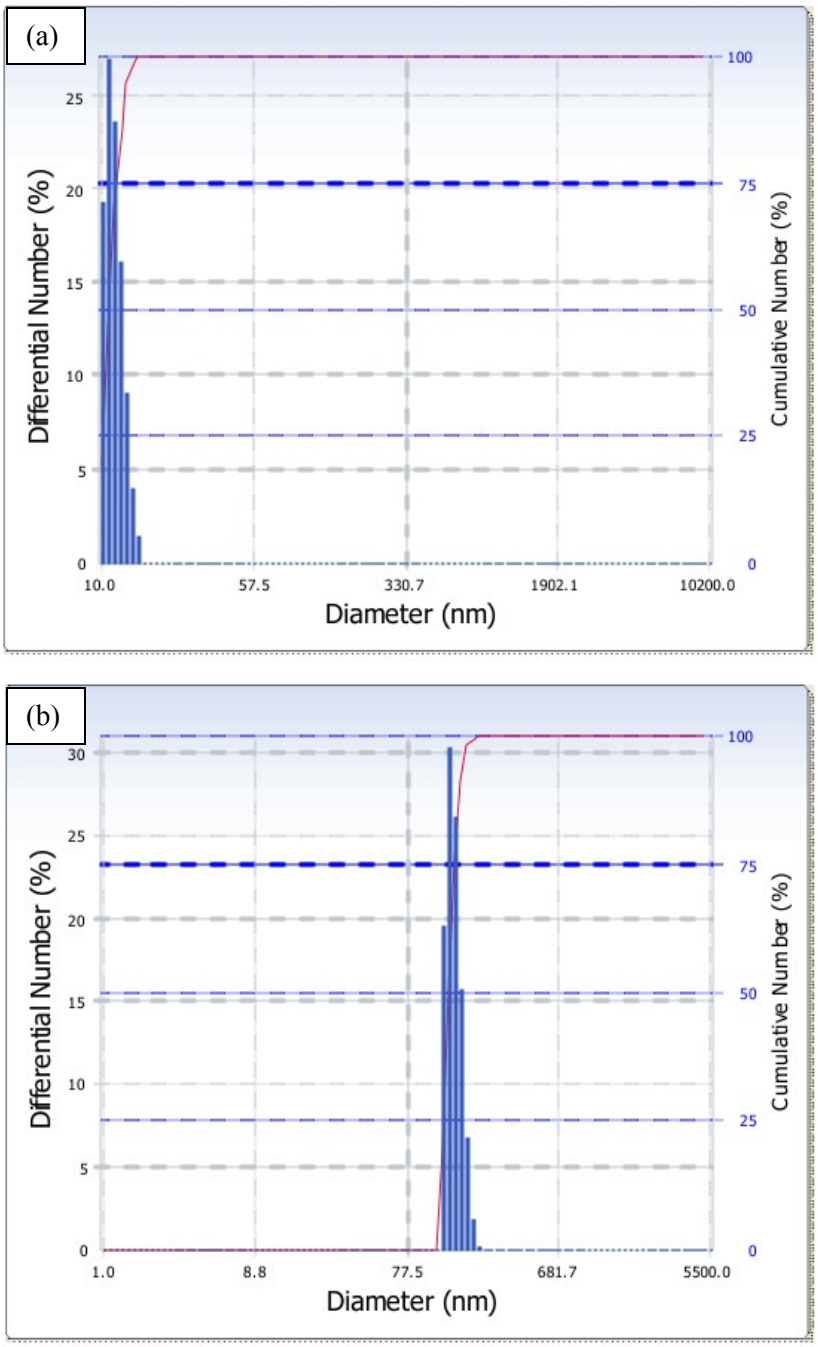

Fig. S11 Dynamic light scattering (DLS) data of (a) **PCS1** in CH_3CN and (b) **PCS1** in CH_3CN with 80% of water fraction.

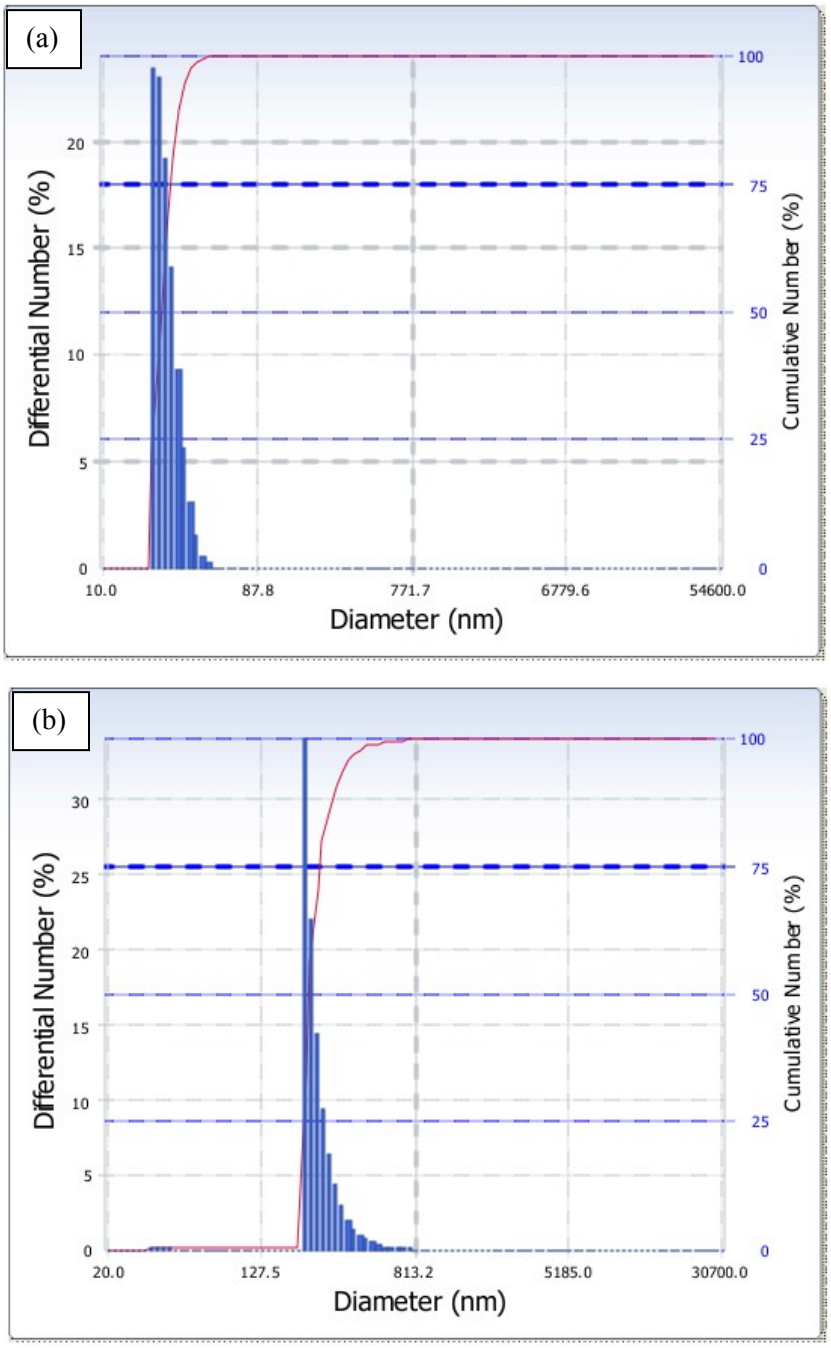

Fig. S12 Dynamic light scattering (DLS) data of (a) **PCS2** in DMSO and (b) **PCS2** in DMSO with 60% of water fraction.

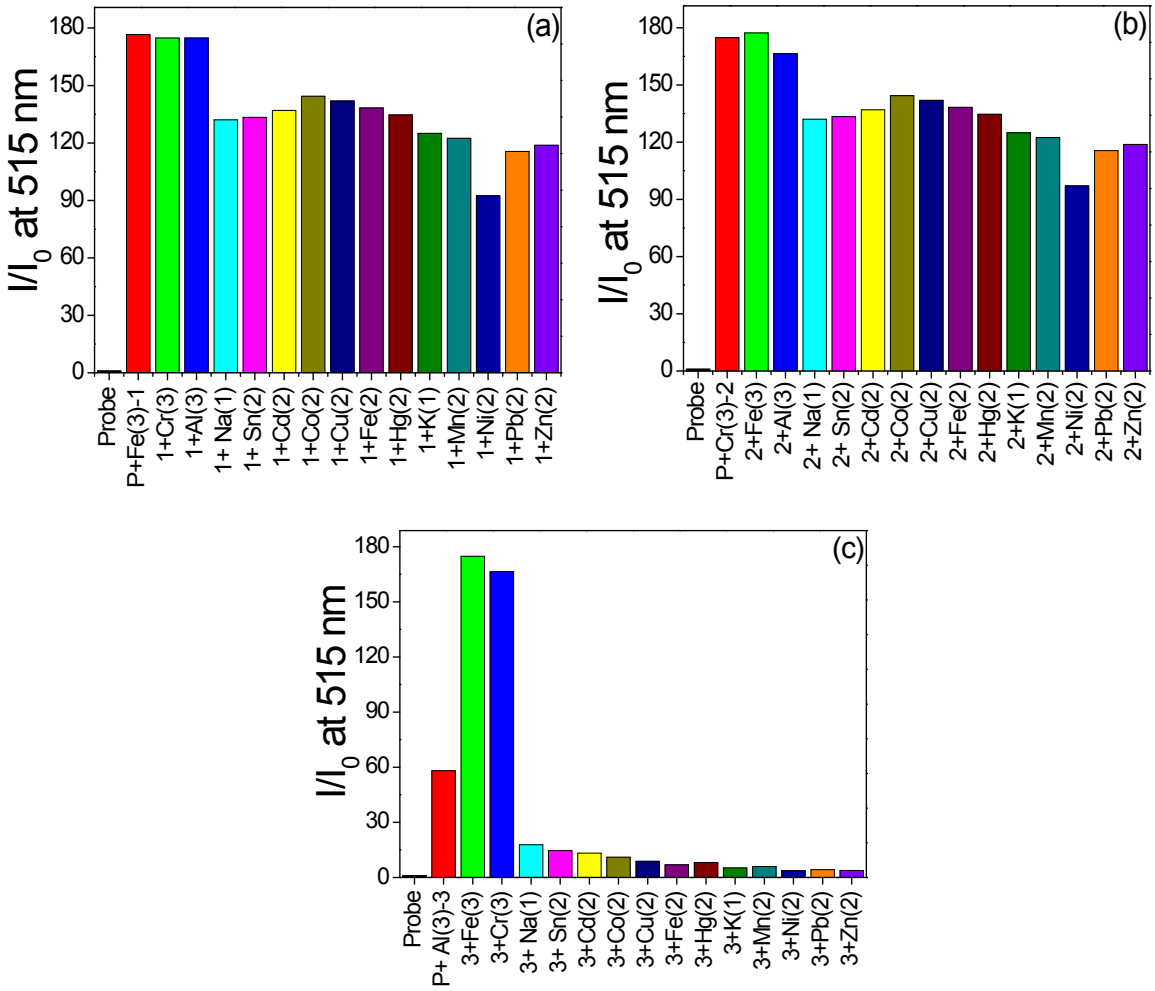

Fig. S13 (a-c) Histograms of **PCS**---M^{3+} (20 μM of M= Fe/ Cr/ Al) in presence of different metal ions (20 μM).

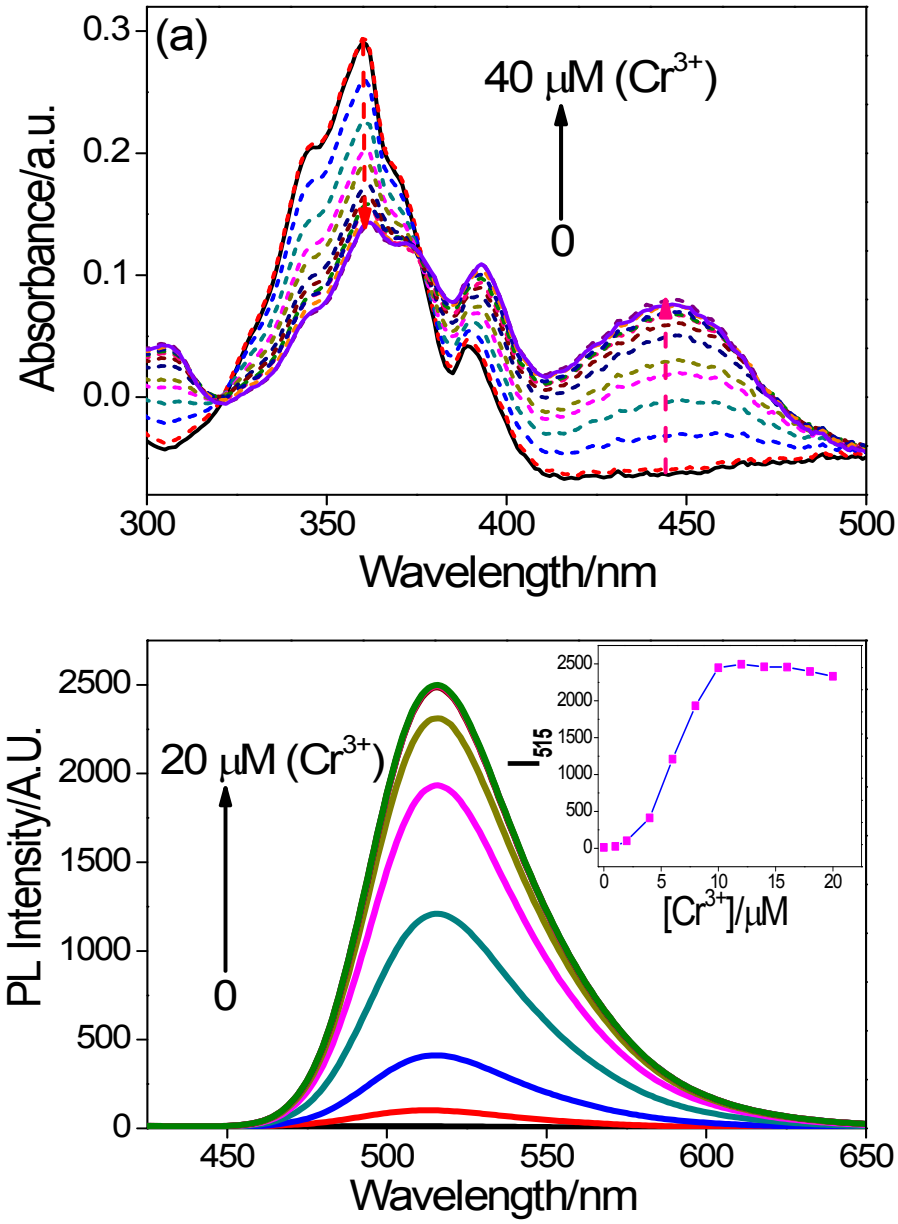

Fig. S14 (a) UV-Vis and (b) PL spectral titrations of **PCS1** (20 μM in CH_3CN) with 0-40 μM and 0-20 μM of Cr^{3+} ions in H_2O, respectively; PL Inset: Intensity changes as a function of Cr^{3+} concentration.

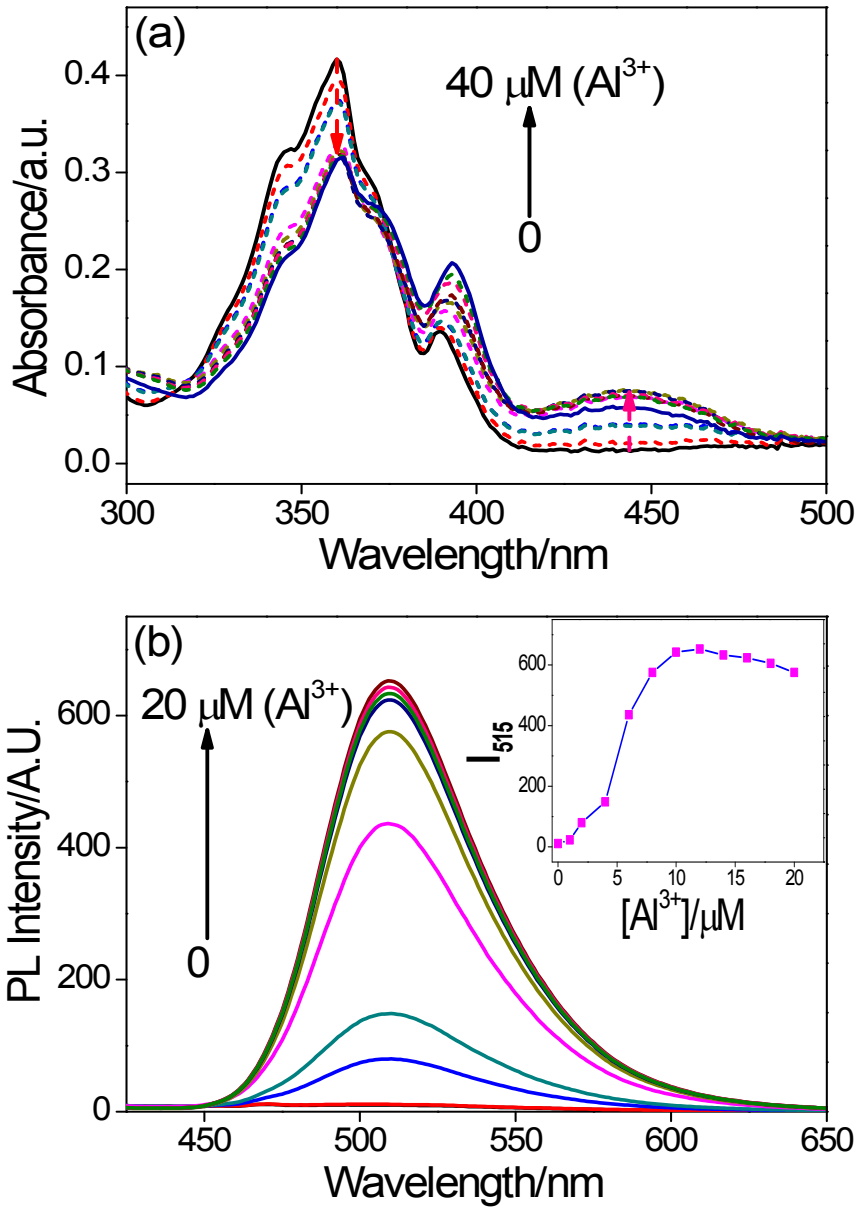

Fig. S15 (a) UV-Vis and (b) PL spectral titrations of **PCS1** (20 μM in CH_3CN) with 0-40 μM and 0-20 μM of Al^{3+} ions in H_2O, respectively; PL Inset: Intensity changes as a function of Al^{3+} concentration.

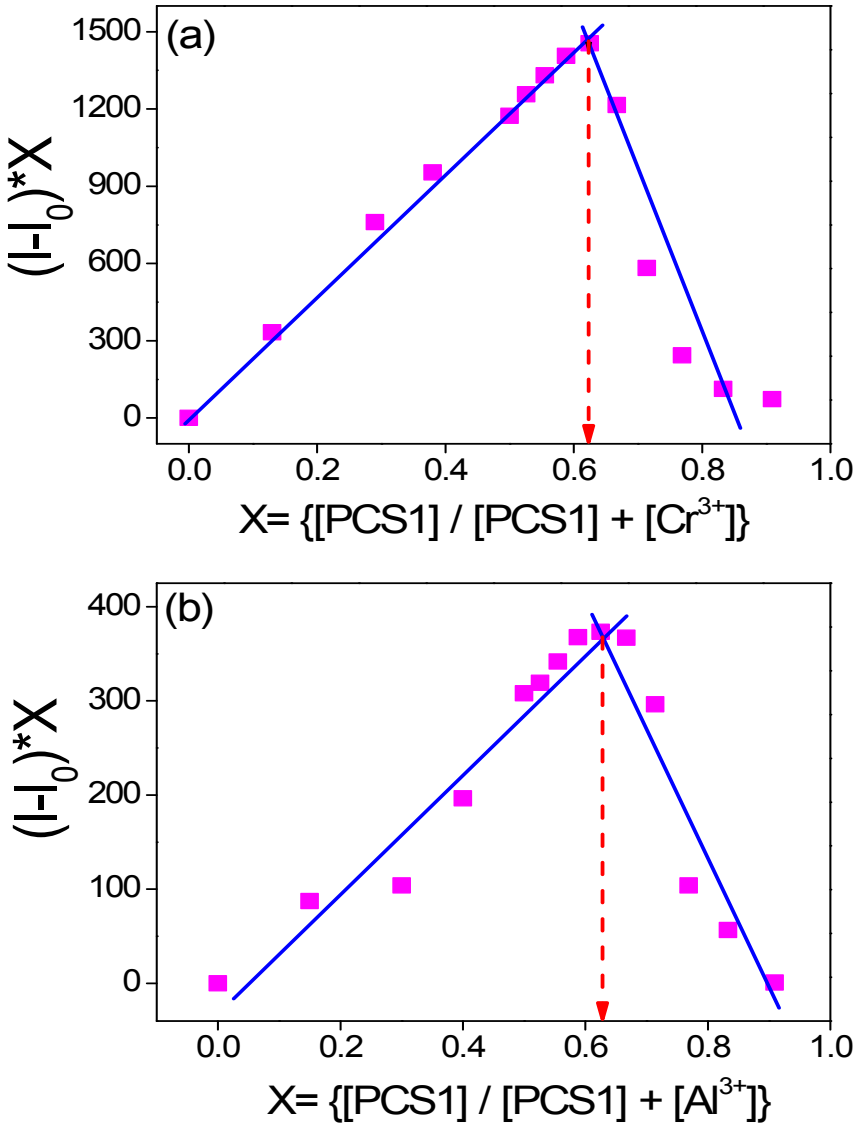

Fig. S16 (a, b) Job's plots (based on PL intensity changes) between X *vs* $(I-I_0)*X$, representing 2:1 [**PCS1**---Cr^{3+} (0.621) and **PCS1**---Al^{3+} (X = 0.628)] complexes.

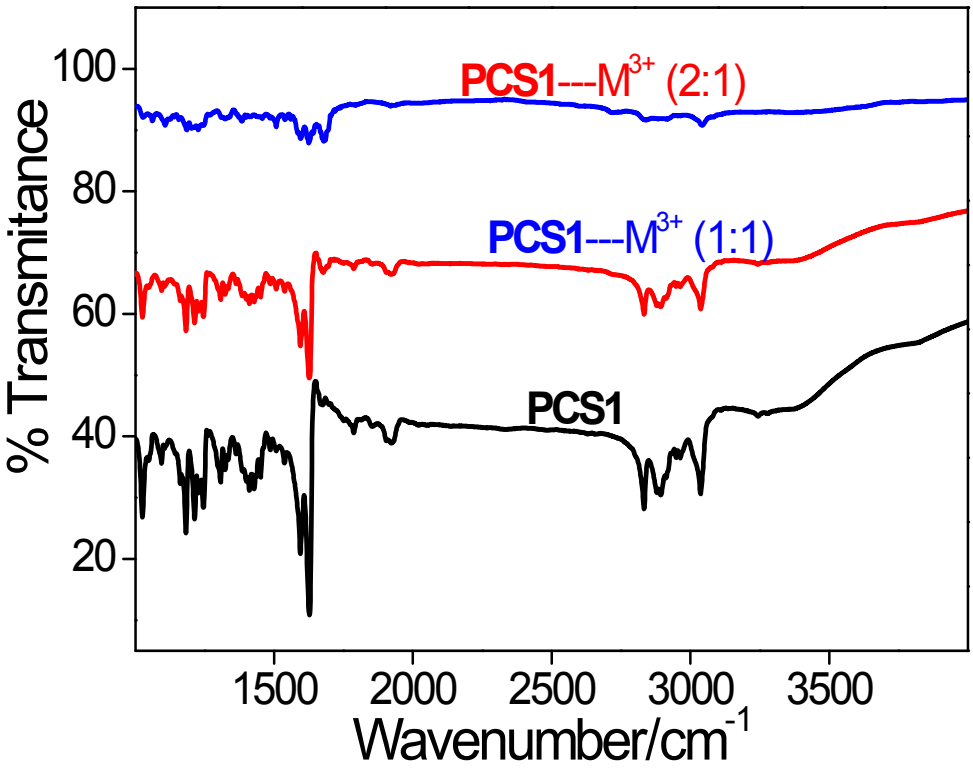

Fig. S17 FTIR spectrum of **PCS1---**M^{3+} (1:1 and 2:1 complexes) confirms 2:1 stoichiometry of **PCS1**---M^{3+} (M = Fe/ Cr/ Al) sensor complexes via excimer formation.

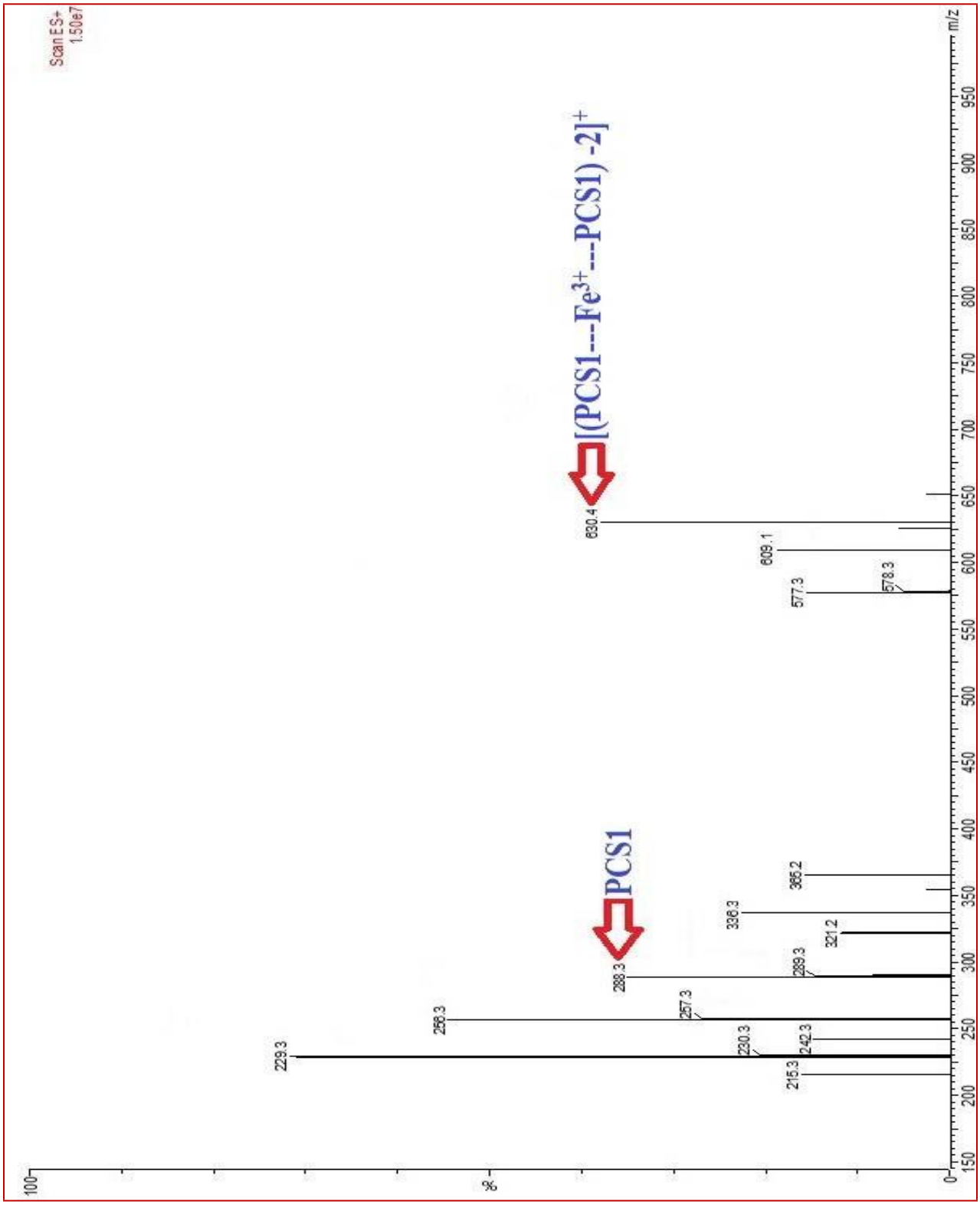

Fig. S18 ESI (+Ve) Mass spectrum of **PCS1**---Fe^{3+} sensor complex, representing 2:1 complex formation.

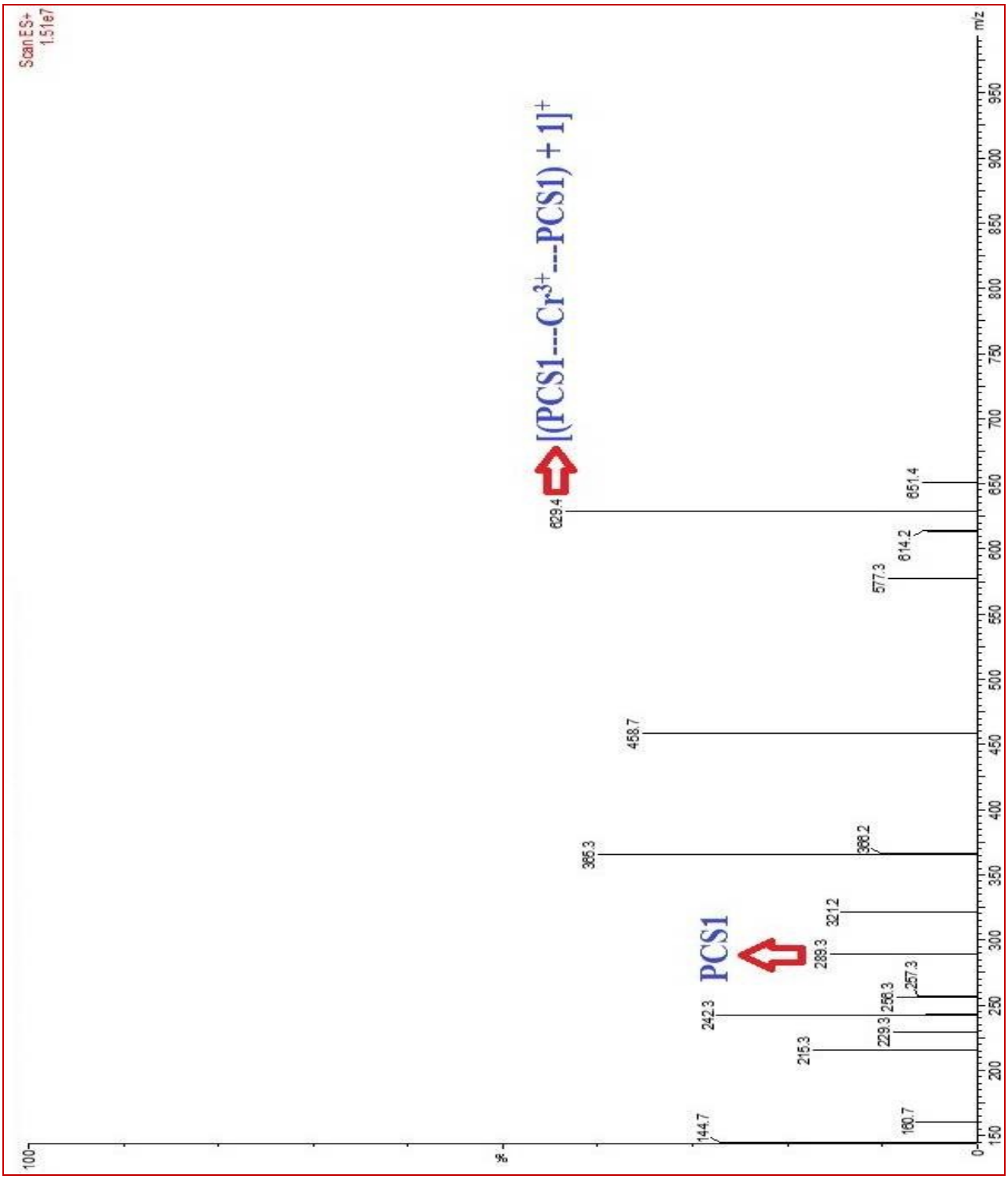

Fig. S19 ESI (+Ve) Mass spectrum of **PCS1**---Cr^{3+} sensor complex, representing 2:1 complex formation.

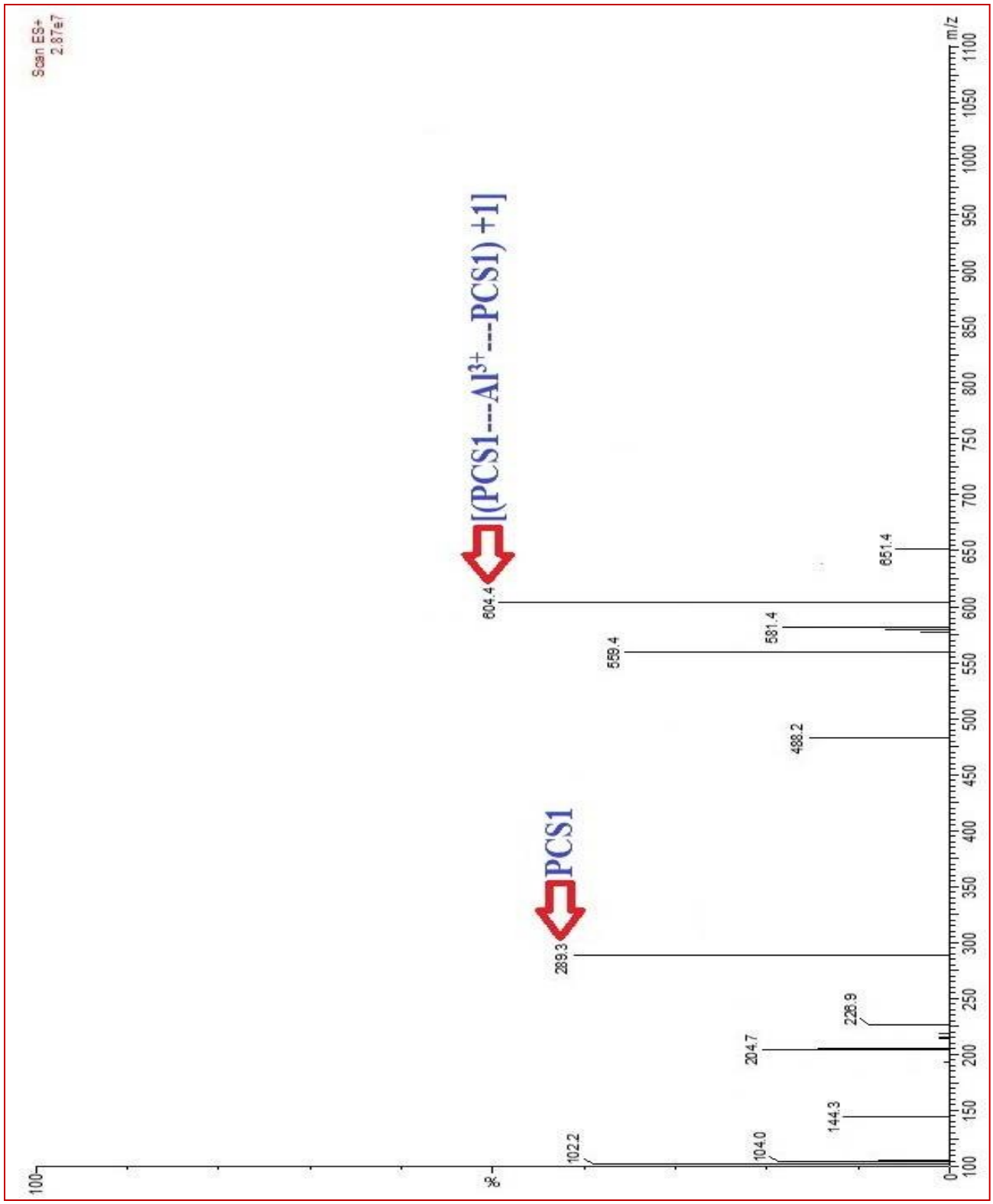

Fig. S20 ESI (+Ve) Mass spectrum of **PCS1**---Al^{3+} sensor complex, representing 2:1 complex formation.

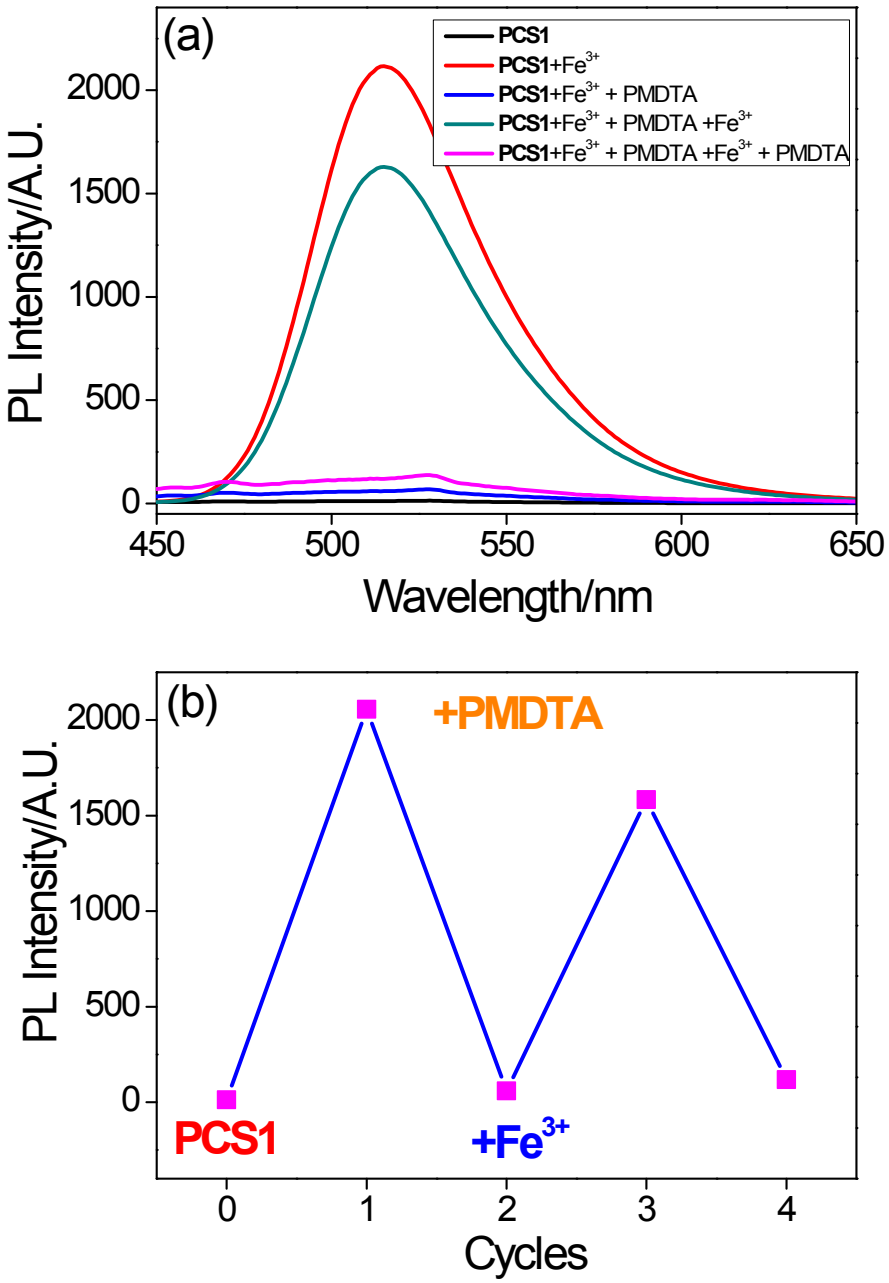

Fig. S21 (a) Sensor reversibility of **PCS1**---Fe^{3+} with PMDTA (b) Reversible cycles with PMDTA.

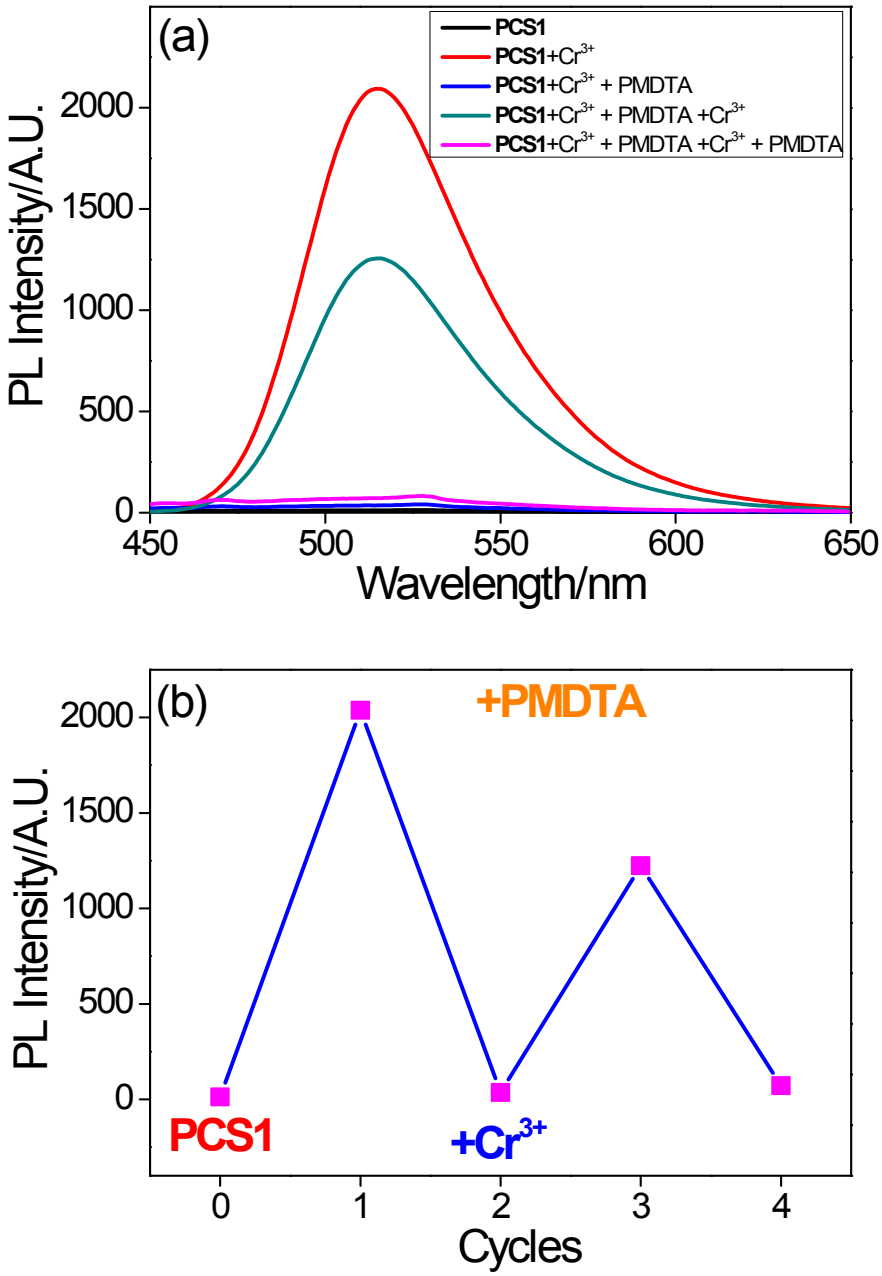

Fig. S22 (a) Sensor reversibility of **PCS1**---Cr^{3+} with PMDTA (b) Reversible cycles with PMDTA.

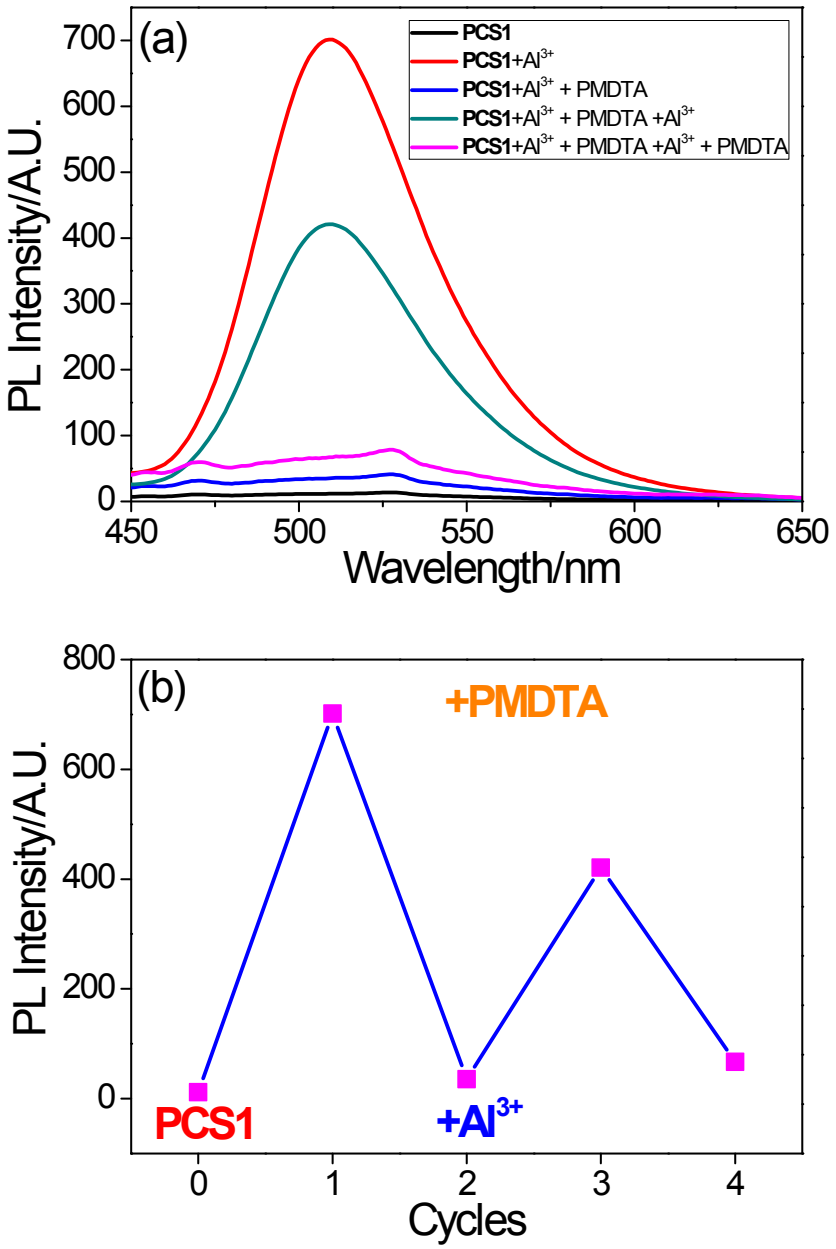

Fig. S23 (a) Sensor reversibility of **PCS1**---Al^{3+} with PMDTA (b) Reversible cycles with PMDTA.

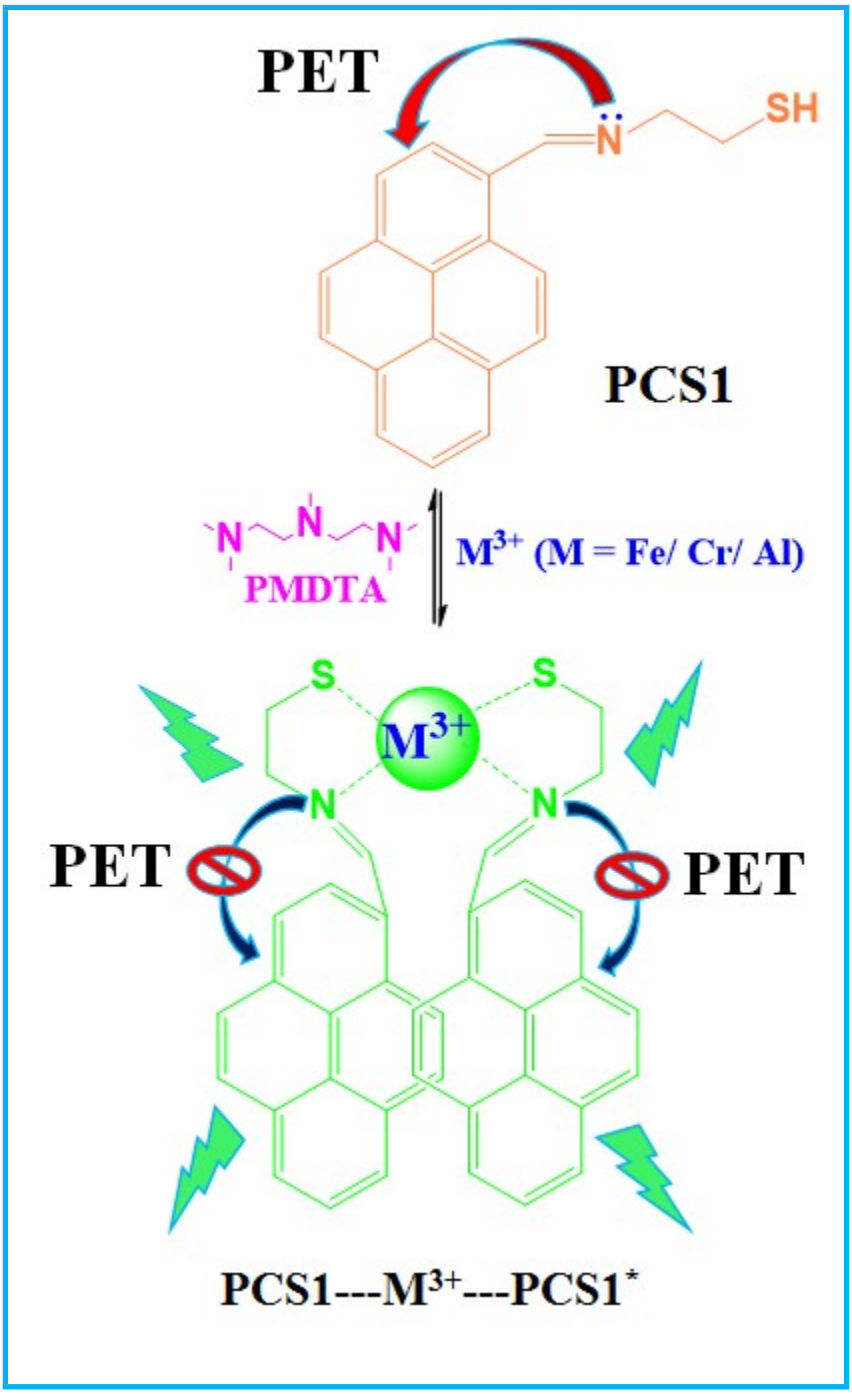

Fig. S24 Schematic illustration of **PCS1**---M^{3+} (M = Fe/ Cr/ Al) induced excimer (**PCS1-PCS1***) formation for sensor selectivity and its reversibility with PMDTA.

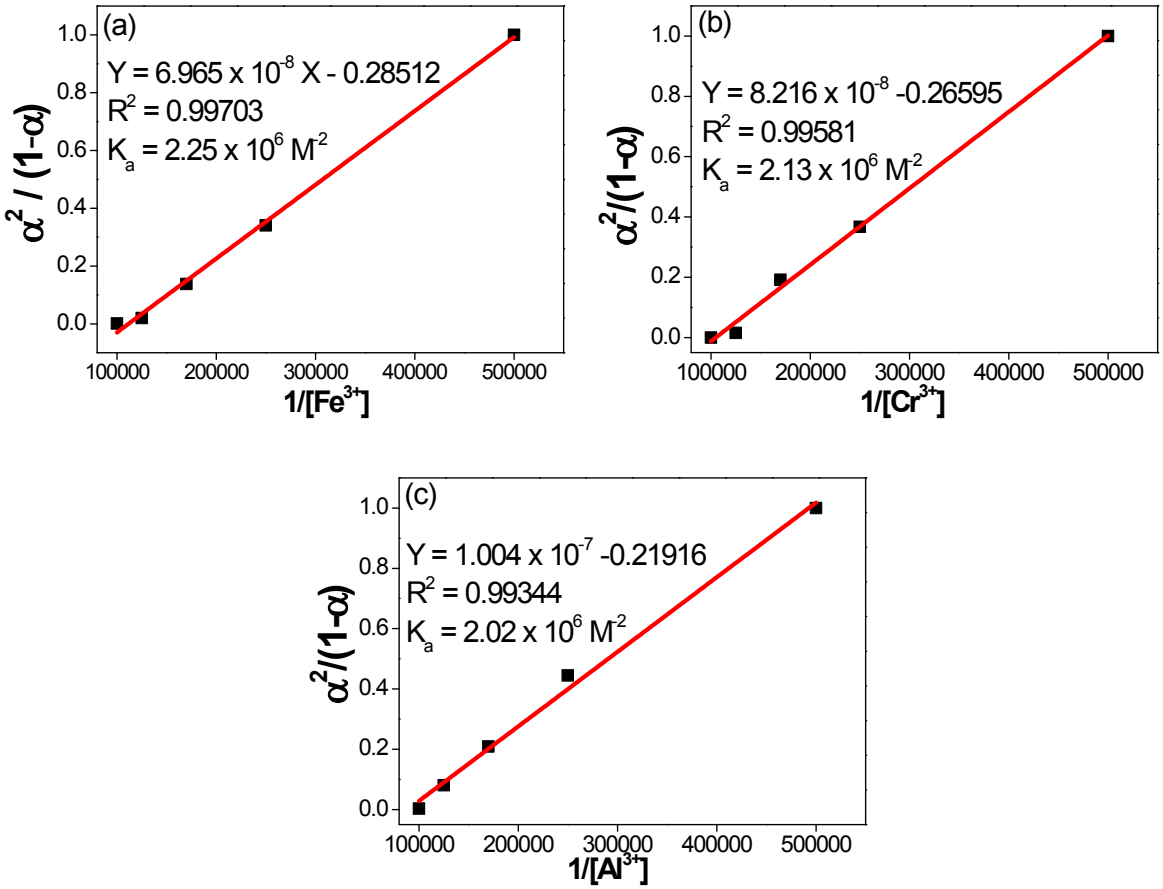

Fig. S25 Association constant calculations by plotting $\alpha^2/(1-\alpha)$ vs $1/M^{3+}$ (M = Fe/ Cr / Al) with linear fitting as well to find out the binding constant of (a) **PCS1**---Fe^{3+} (b) **PCS1**---Cr^{3+} (c) **PCS1**---Al^{3+}; where α = F-F0/F1-F0, F = PL intensity at 515 nm at any given concentration of M^{3+}, F0 = PL maxima in presence of M^{3+}, and F1 = PL maxima in the absence of M^{3+}.

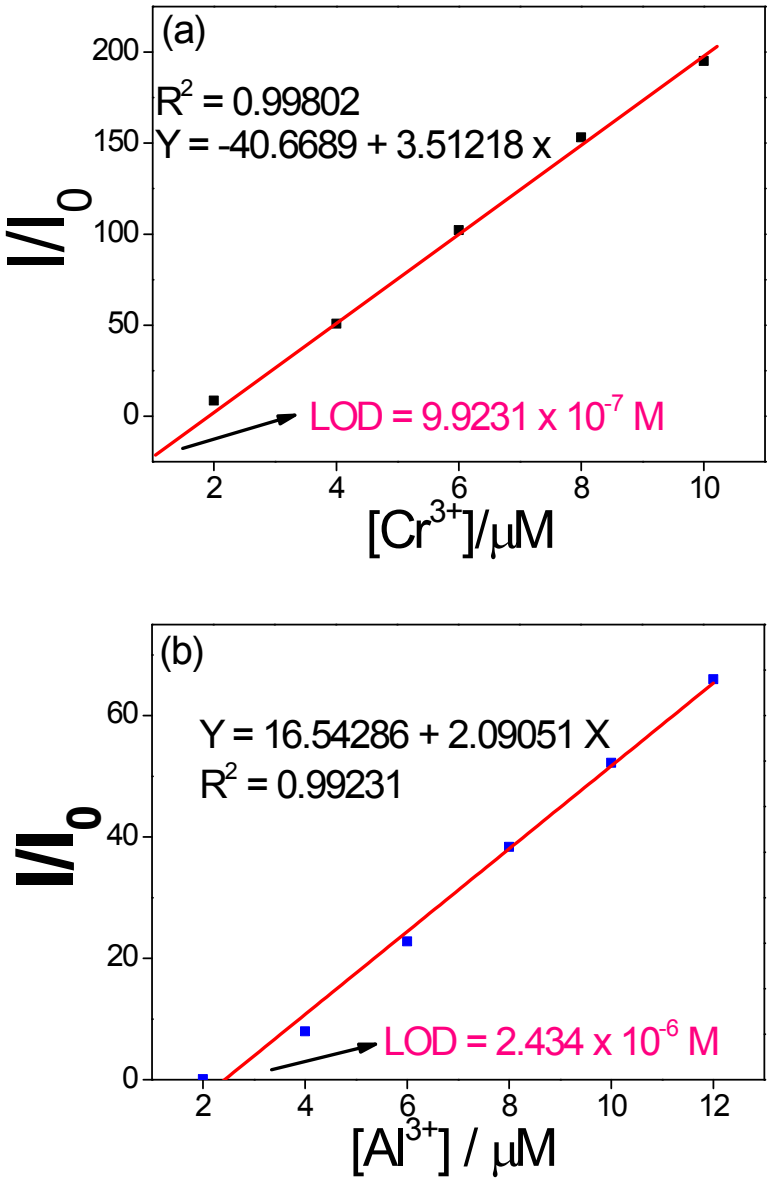

Fig. S26 Standard deviation and linear fitting calculations for detection limits of (a) **PCS1**---Cr^{3+} (b) **PCS1**---Al^{3+} based on PL intensity changes at 515 nm.

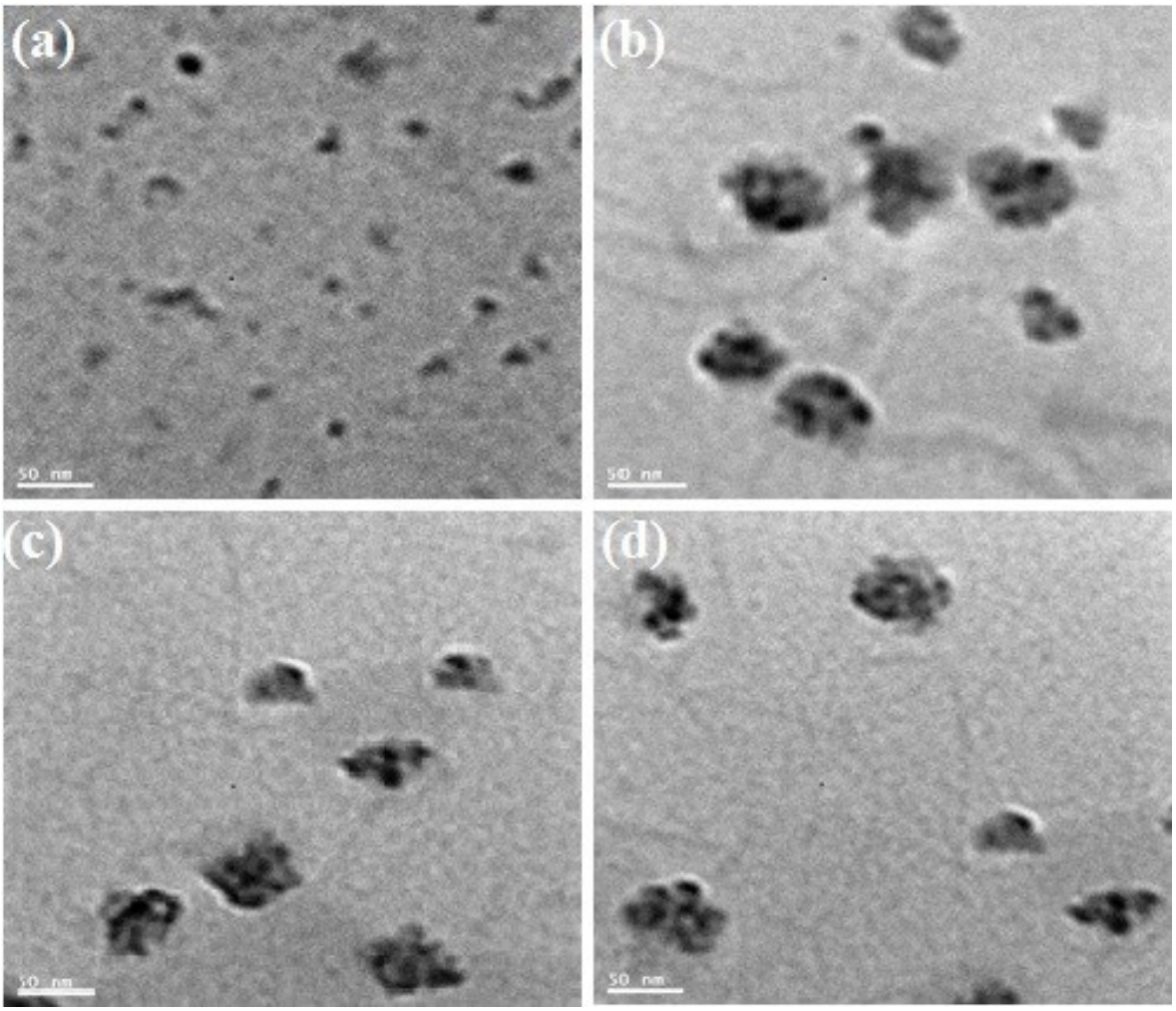

Fig. S27 TEM images of (a) **PCS1** (b) **PCS1**---Fe^{3+} (c) **PCS1**---Cr^{3+} (d) **PCS1**---Al^{3+}.

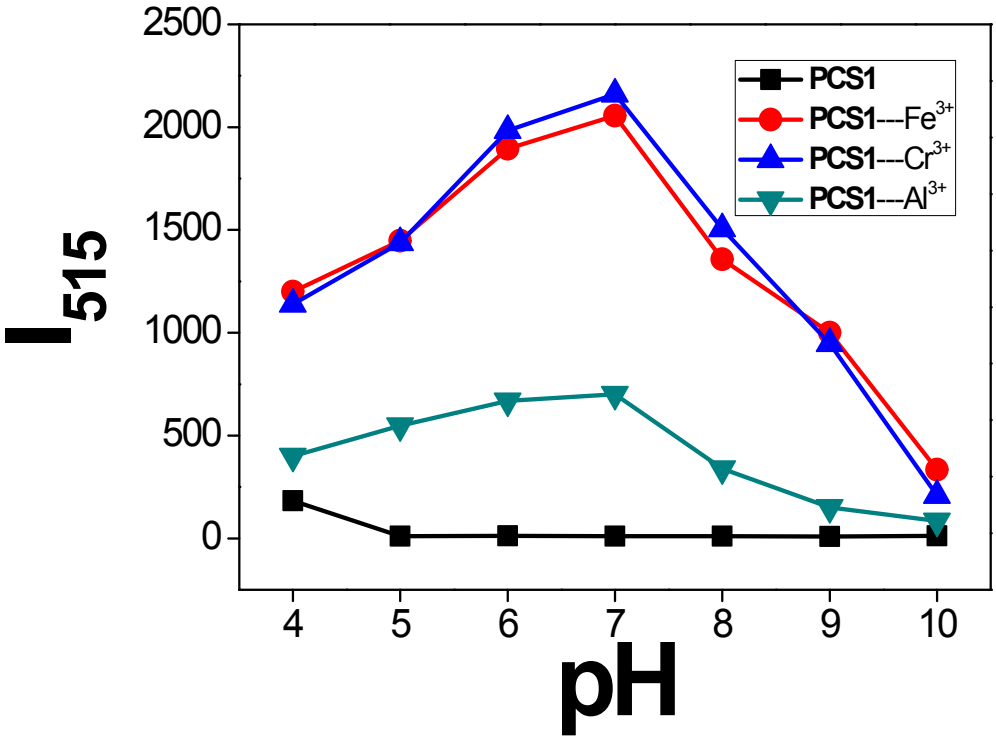

Fig. S28 pH effect on **PCS1** and **PCS1---**M^{3+} (M = Fe/ Cr/ Al) sensor system.

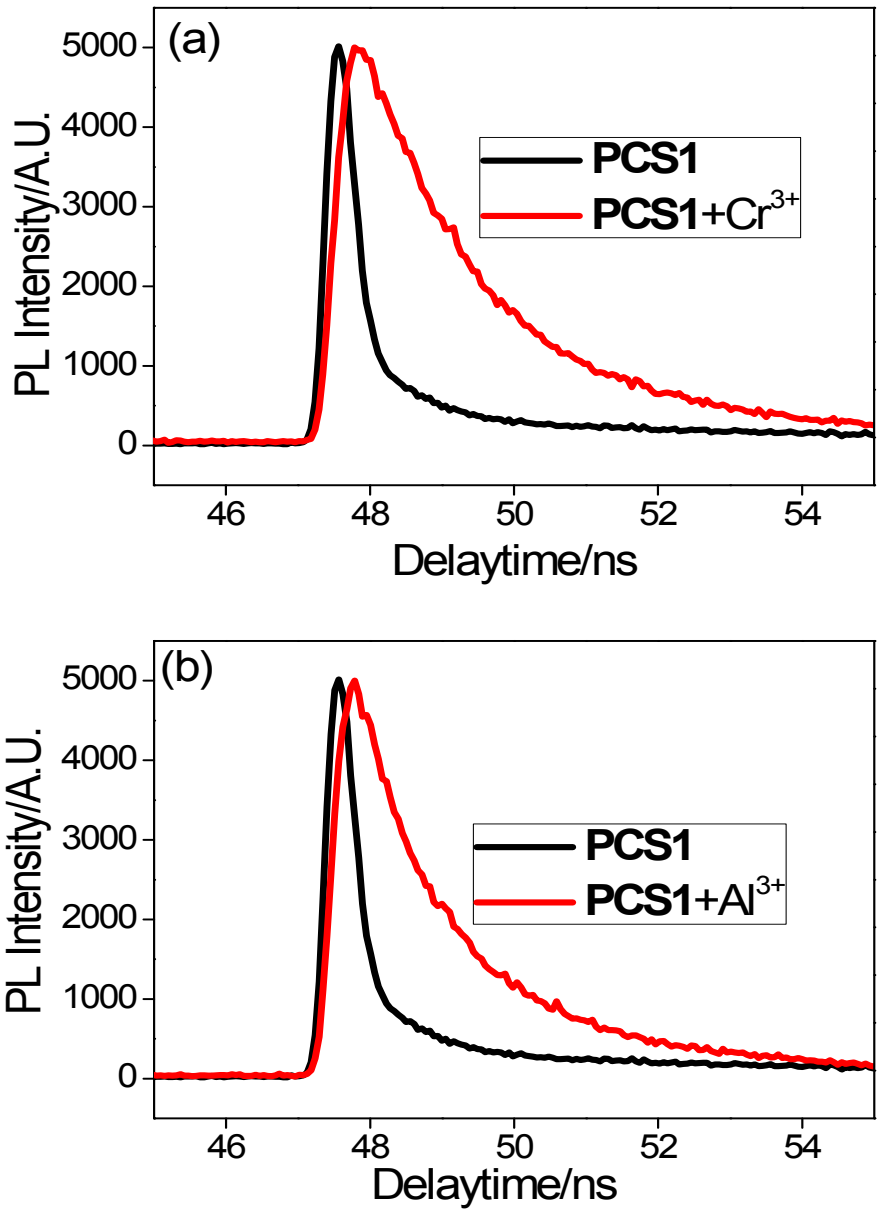

Fig. S29 TRPL spectra of (a) **PCS1** and **PCS1**---Cr^{3+}; (b) **PCS1** and **PCS1**---Al^{3+}.

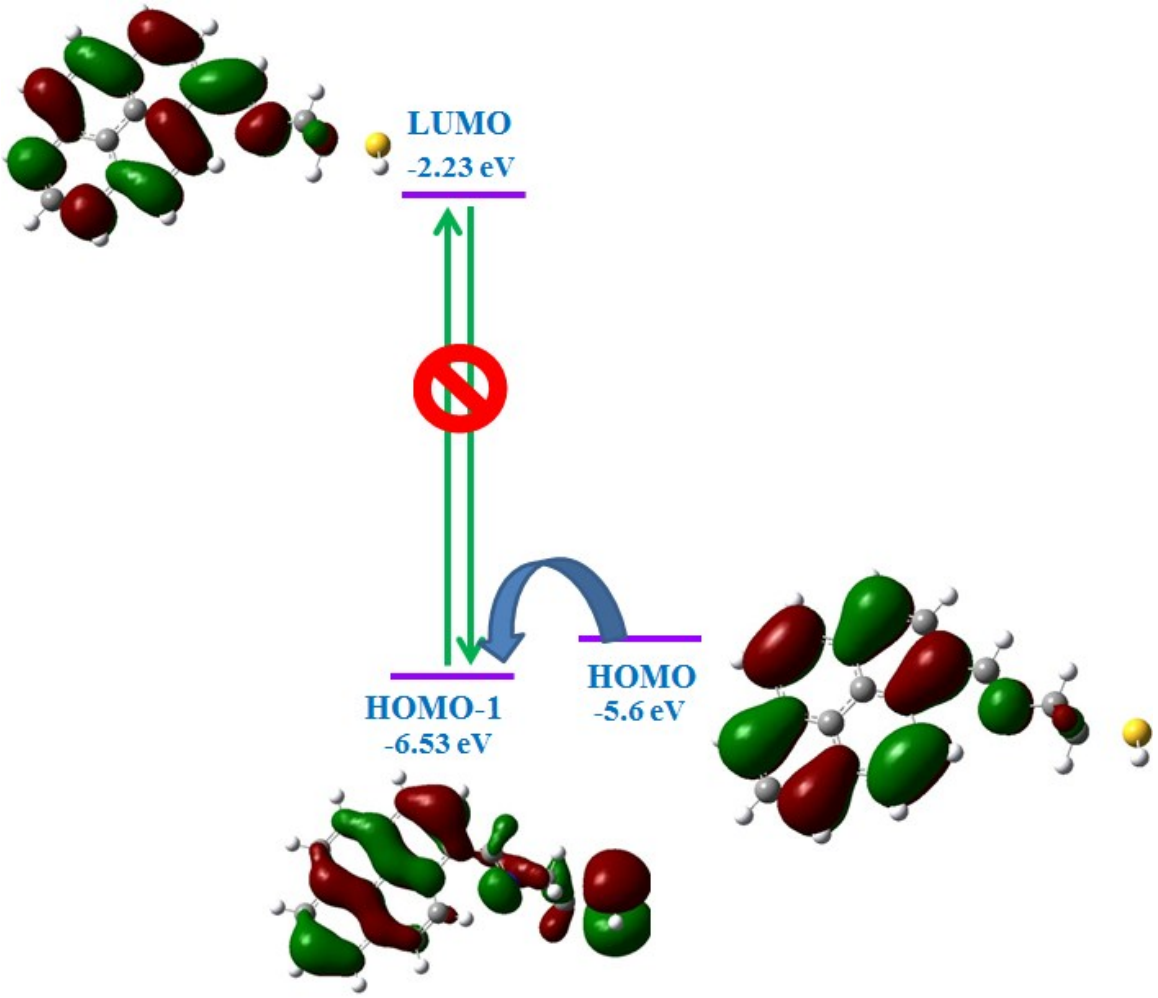

Fig. S30 Frontier Molecular Orbital diagram of **PCS1** in gas phase at B3LYP/LANL2DZ level.

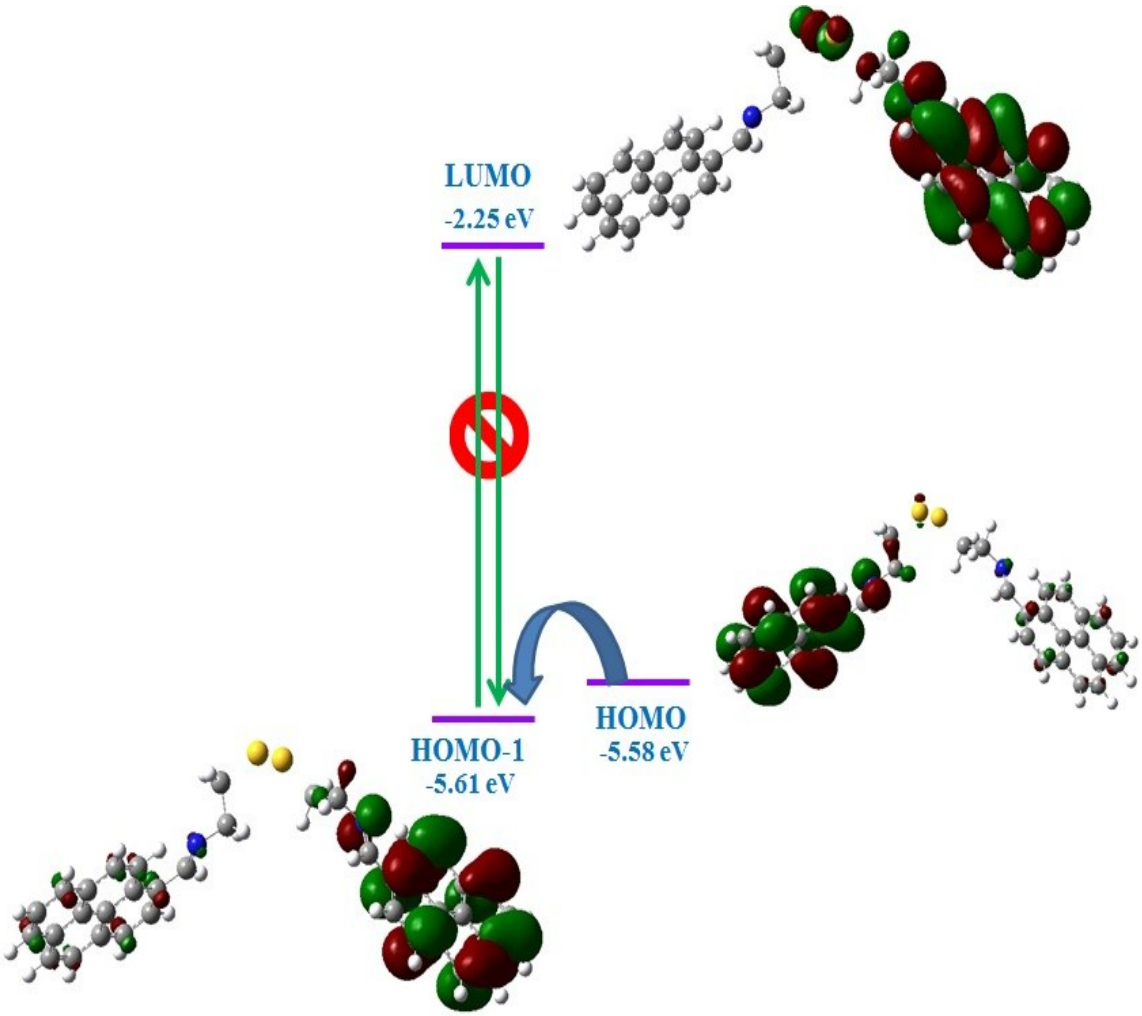

Fig. S31 Frontier Molecular Orbital diagram of **PCS2** in gas phase at B3LYP/LANL2DZ level.

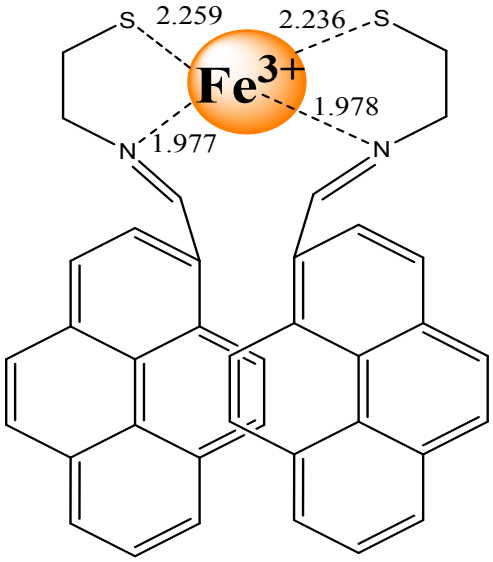

PCS1-PCS1* (Fe^{3+})

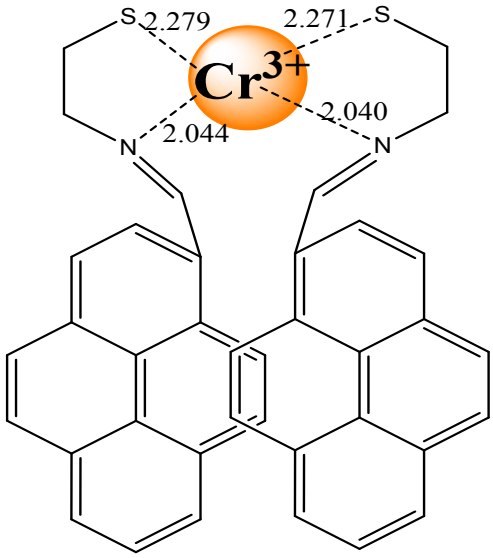

PCS1-PCS1* (Cr^{3+})

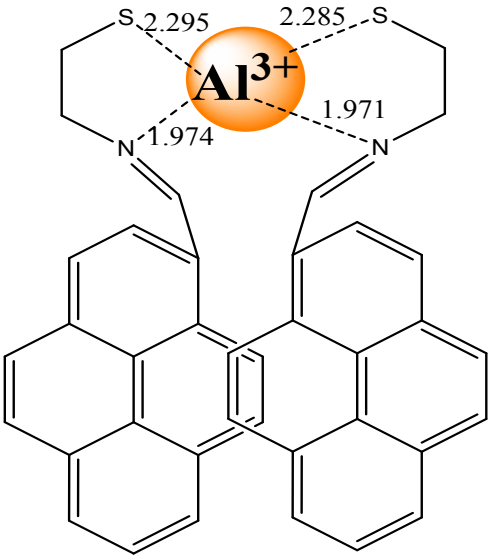

PCS1-PCS1*(Al^{3+})

Fig. S32 The bond distances (Å) between M^{3+}---O and M^{3+}---N of **PCS1**---M^{3+} complexes shown in schematic representation of optimized sensor complexes (M = Fe/ Cr/ Al).

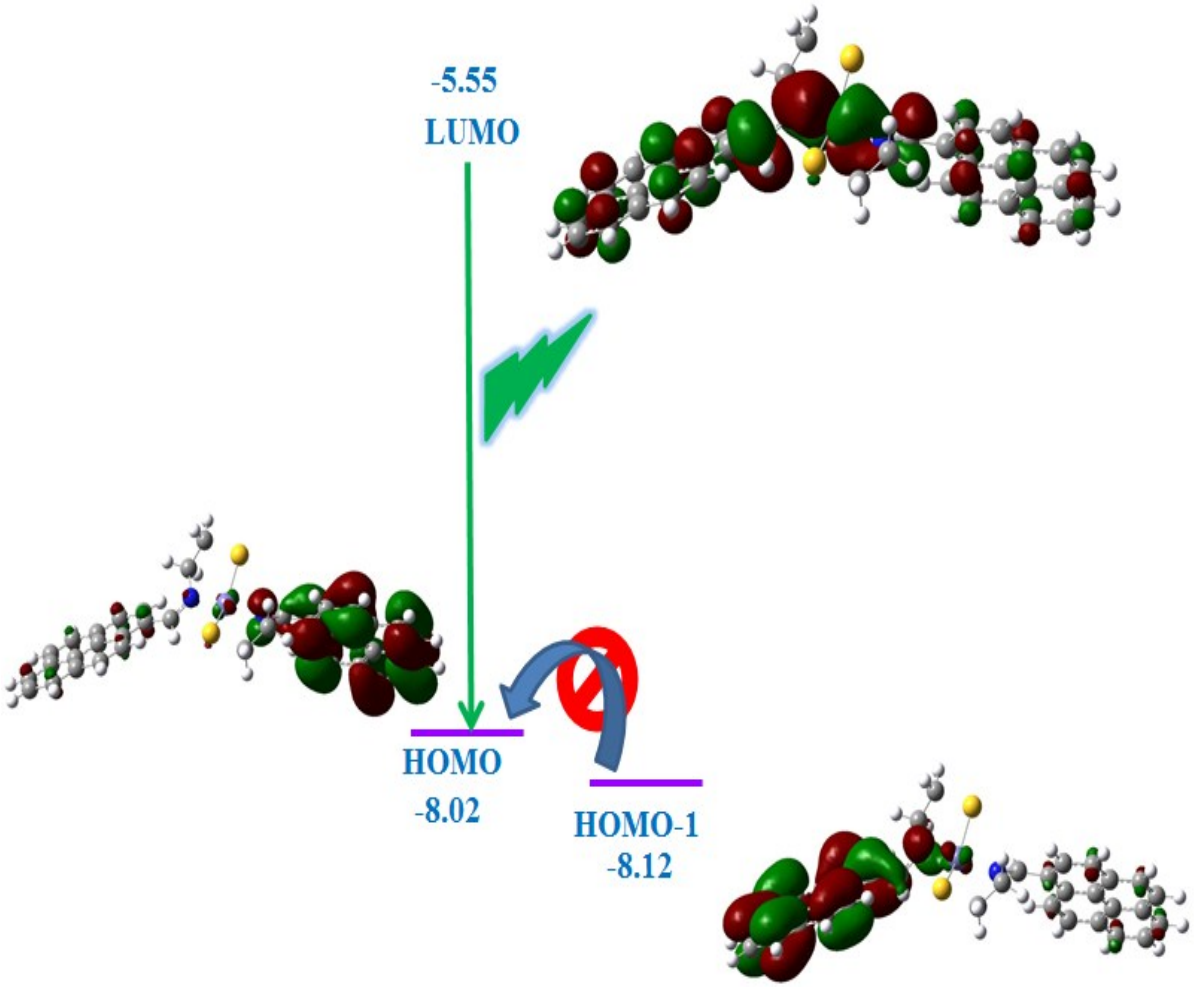

Fig. S33 Frontier Molecular Orbital diagram of [**PCS1**---Fe]$^{+}$ in gas phase at B3LYP/LANL2DZ level (Note: **PCS1**---Fe –β PET Unrestricted).

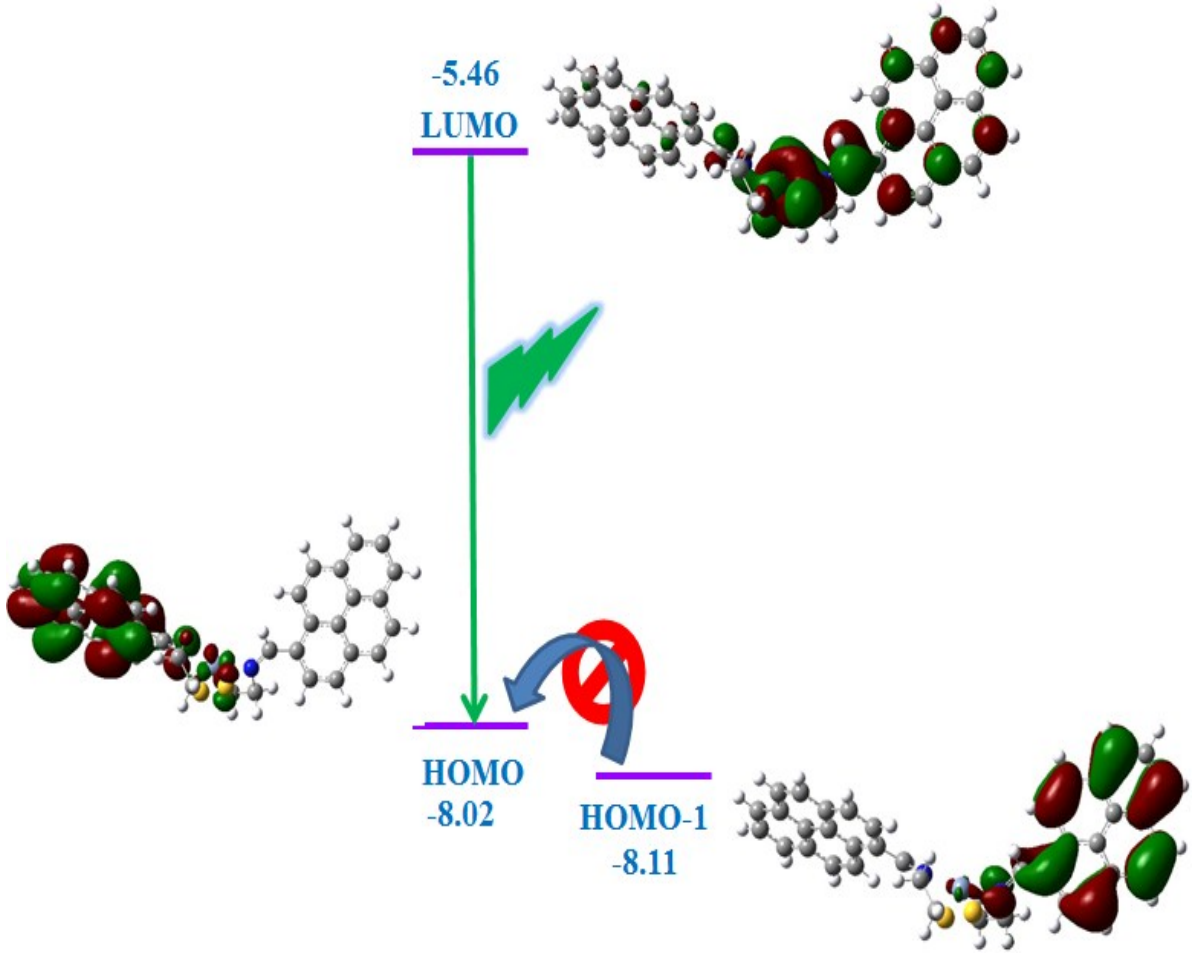

Fig. S34 Frontier Molecular Orbital diagram of [**PCS1**---Cr]$^{+}$ in gas phase at B3LYP/LANL2DZ level (Note: **PCS1**---Cr–β PET Unrestricted).

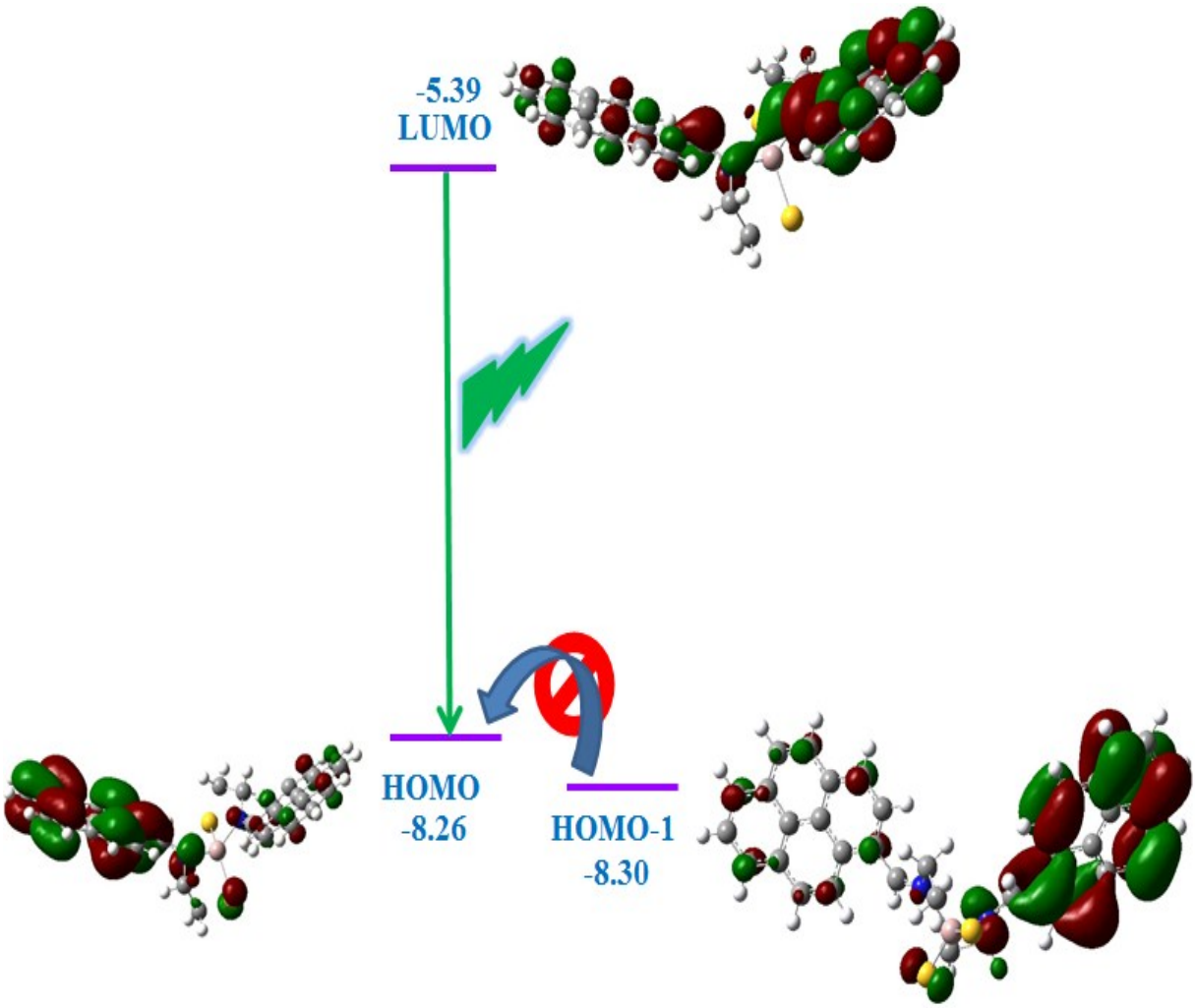

Fig. S35 Frontier Molecular Orbital diagram of [**PCS1**---Al]$^{+}$ in gas phase at B3LYP/LANL2DZ level.

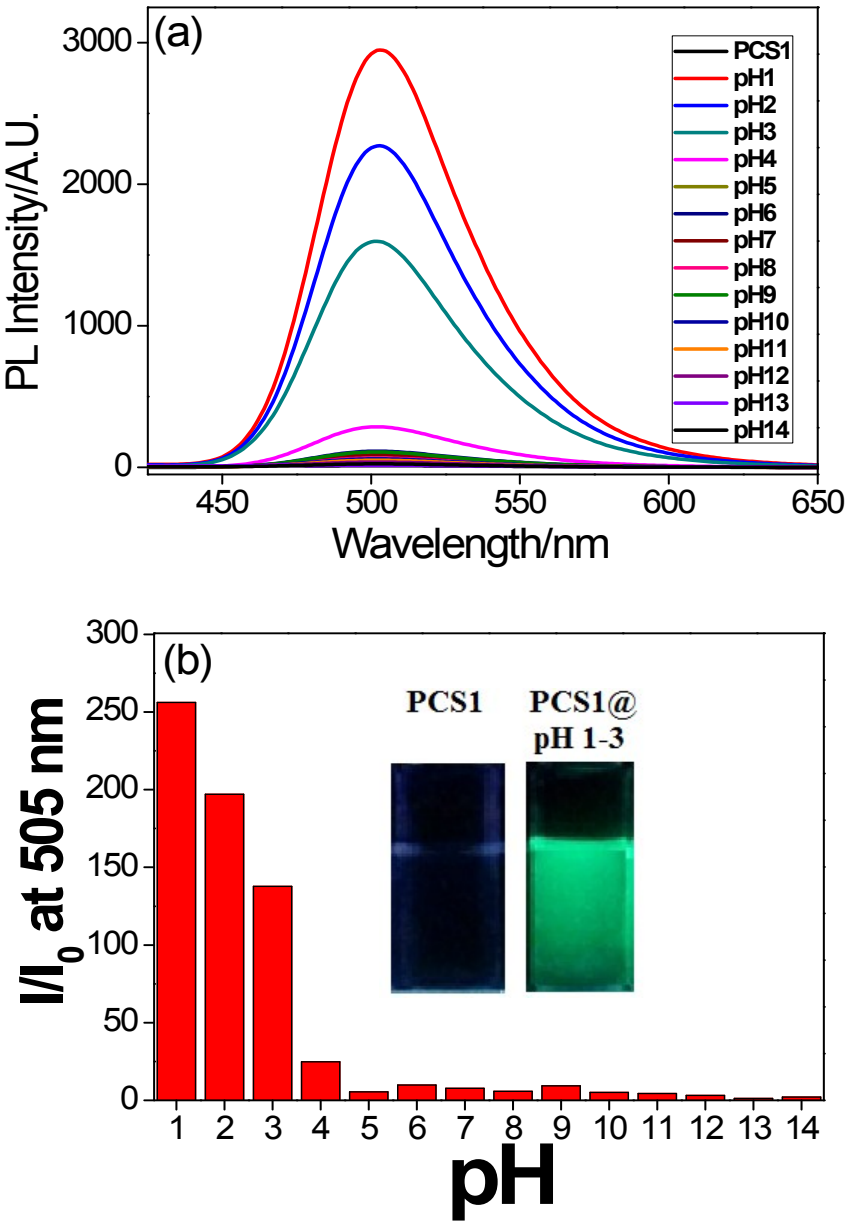

Fig. S36 (a) PL spectra of **PCS1** (950 μL; 20 μM in CH_3CN) with 50 μL of pH (1-14; 1 M) solution; (b) Bar graph of **PCS1** with respective pH solutions; Inset: Acidic pH sensor responses of **PCS1** visualized under UV-irradiations (λ = 365 nm).

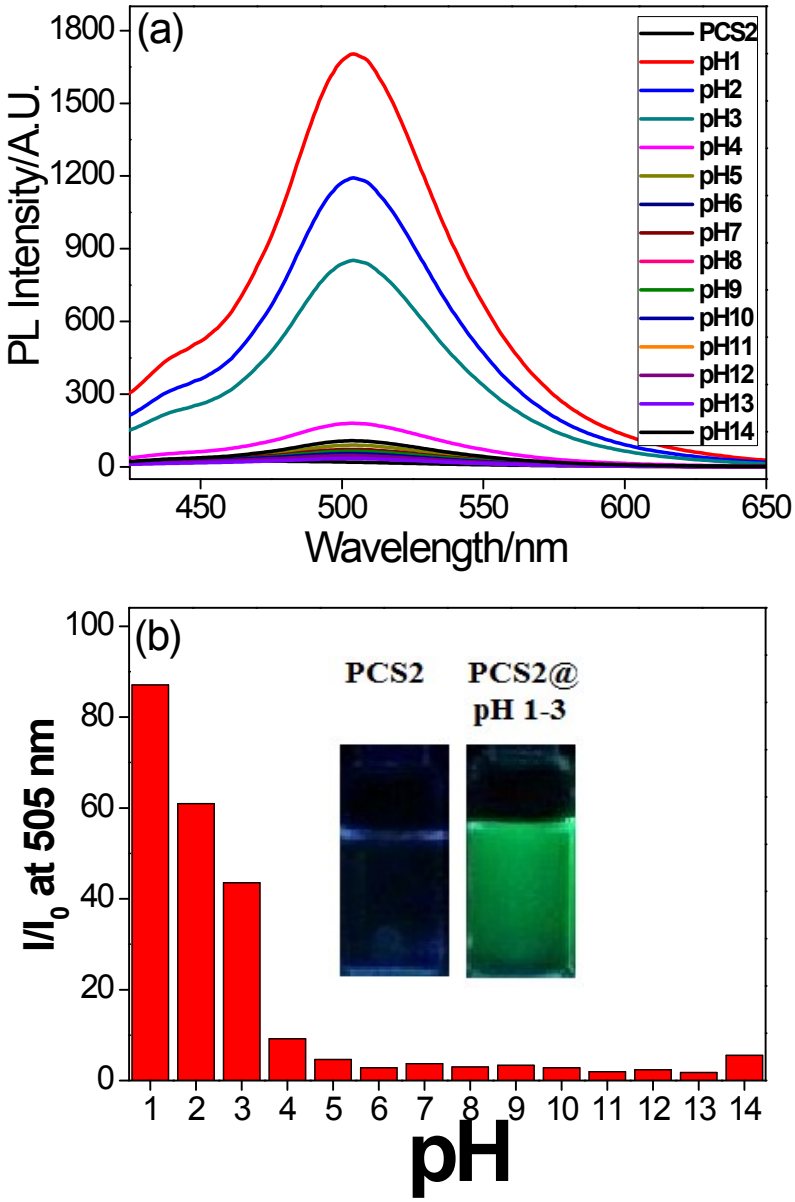

Fig. S37 (a) PL spectra of **PCS2** (950 μL; 20 μM in CH_3CN) with 50 μL of pH (1-14; 1 M) solution; (b) Bar graph of **PCS2** with respective pH solutions; Inset: Acidic pH sensor responses of **PCS2** visualized under UV-irradiations (λ = 365 nm).

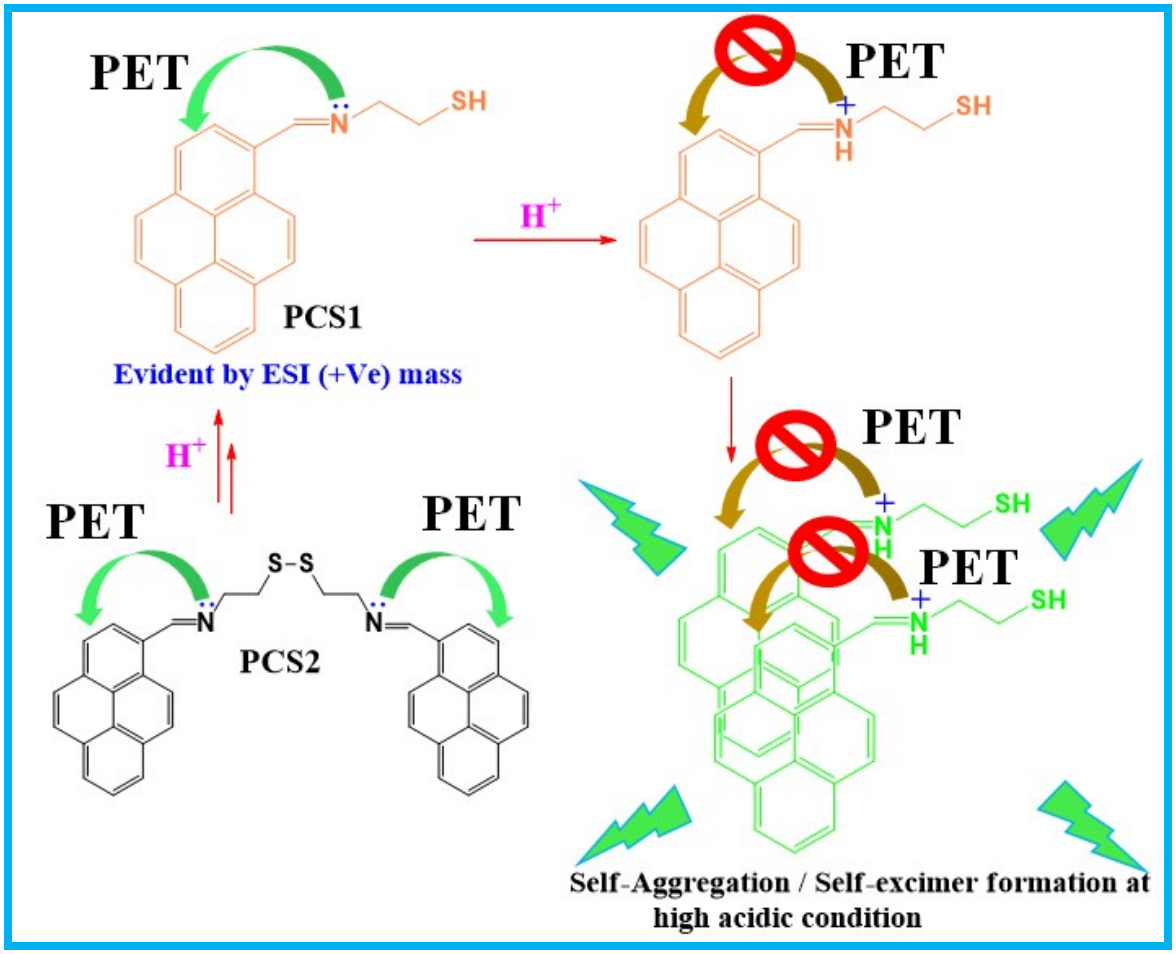

Fig. S38 Possible PET based proposed mechanism for highly acidic pH sensing of **PCS1** and **PCS2**.

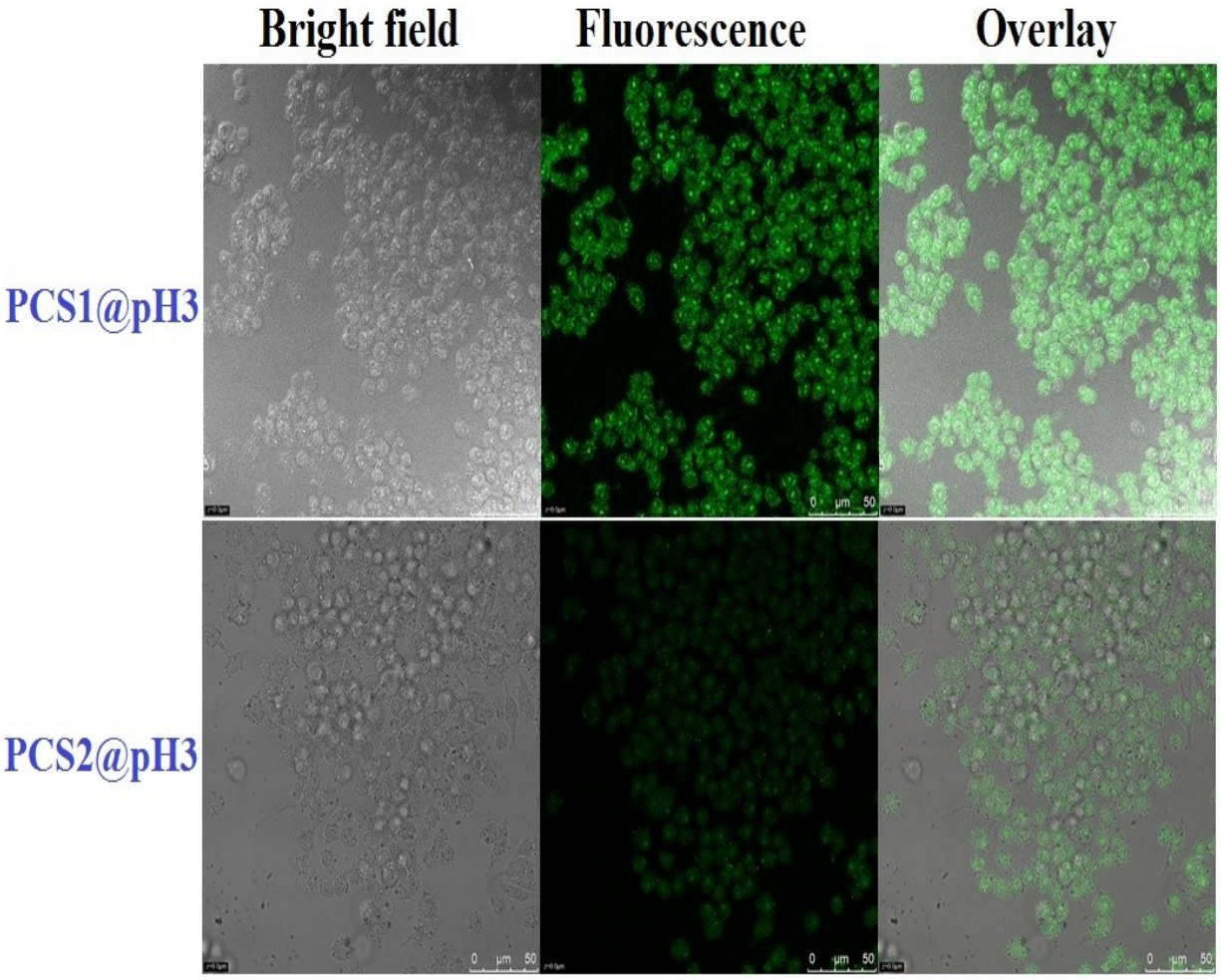

Fig. S39 Fluorescence images of Raw264.7 cells treated with **PCS1** and **PCS2** at pH 3 (incubated for 50 minutes). Bright Field image (Left); Fluorescence image (middle); Merged image (right). The scale bar is 50 μM.

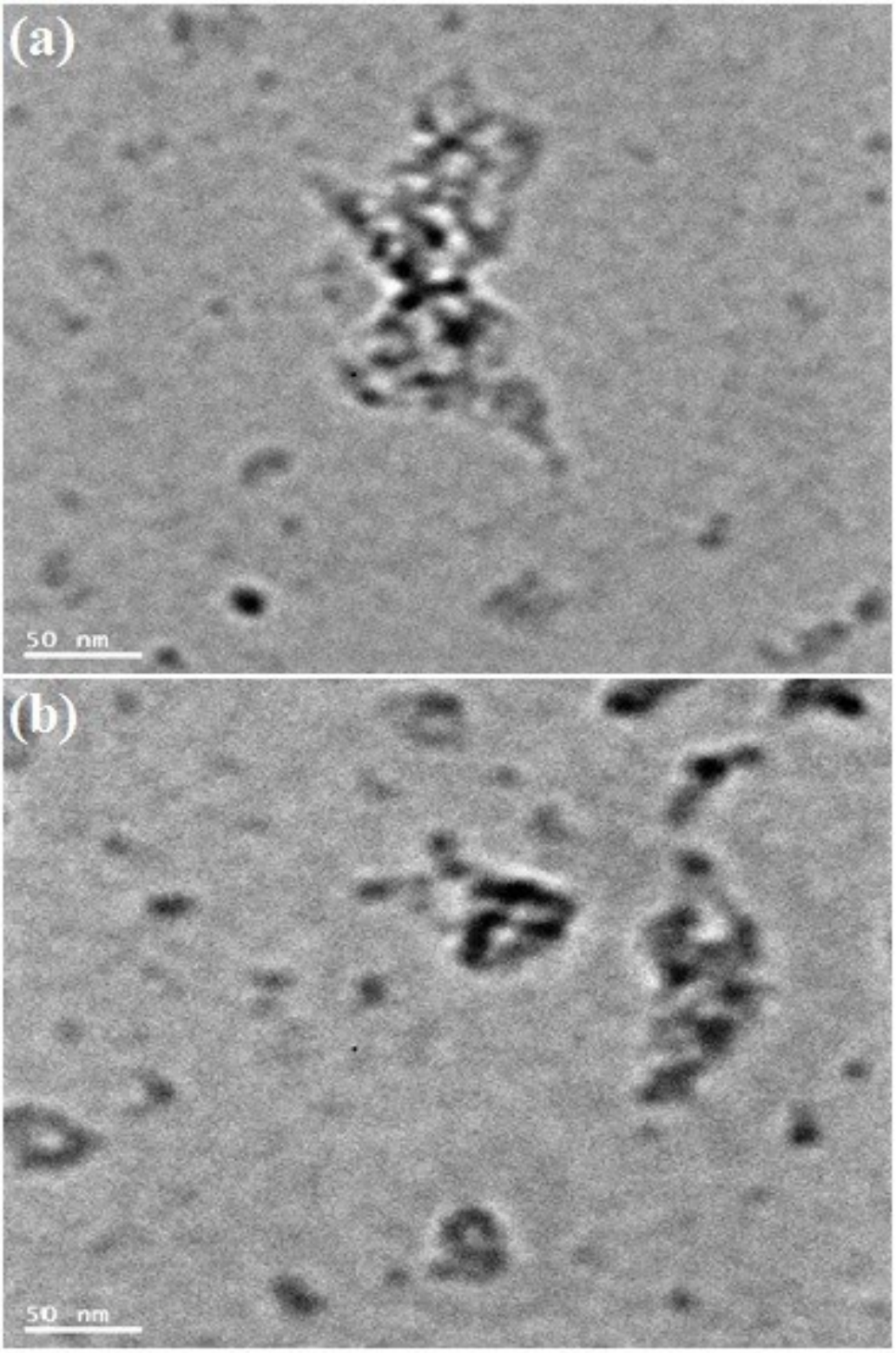

Fig. S40 TEM images of (a) **PCS1** at pH = 3.0 and (b) **PCS2** at pH =3.0.

Table S1. Time-resolved fluorescence decay constants of **PCS1** and **PCS2**, sensor complexes and their aggregation induced emissions concentrations.

Compound	τ_1(ns)	τ_2(ns)	A_1(%)	A_2(%)	τ_{Avg}(ns)
PCS1 (0%)	9.855	0.3784	60.43	39.57	3.105
PCS1---Fe^{3+}	21.89	1.7514	19.82	80.18	5.74
PCS1---Cr^{3+}	17.87	1.62	18.71	81.29	4.96
PCS1---Al^{3+}	8.29	1.9424	18.44	81.56	4.66
PCS1 (80%)	12.778	2.0132	26.01	73.99	4.813
PCS2 (0%)	3.742	0.2497	31.36	68.64	1.345
PCS2 (60%)	4.614	1.0915	21.70	78.30	1.856
PCS2+HCl	3.72	0.5489	5.43	94.57	0.72